Microscopy Techniques

DOI: 10.1002/anie.201005845

Light Microscopy with Doughnut Modes: A Concept to Detect, Characterize, and Manipulate Individual Nanoobjects

*Tina Züchner, Antonio Virgilio Failla, and Alfred J. Meixner**

Keywords:
higher order laser modes · imaging agents · microscopy · nanotechnology · single-molecule studies

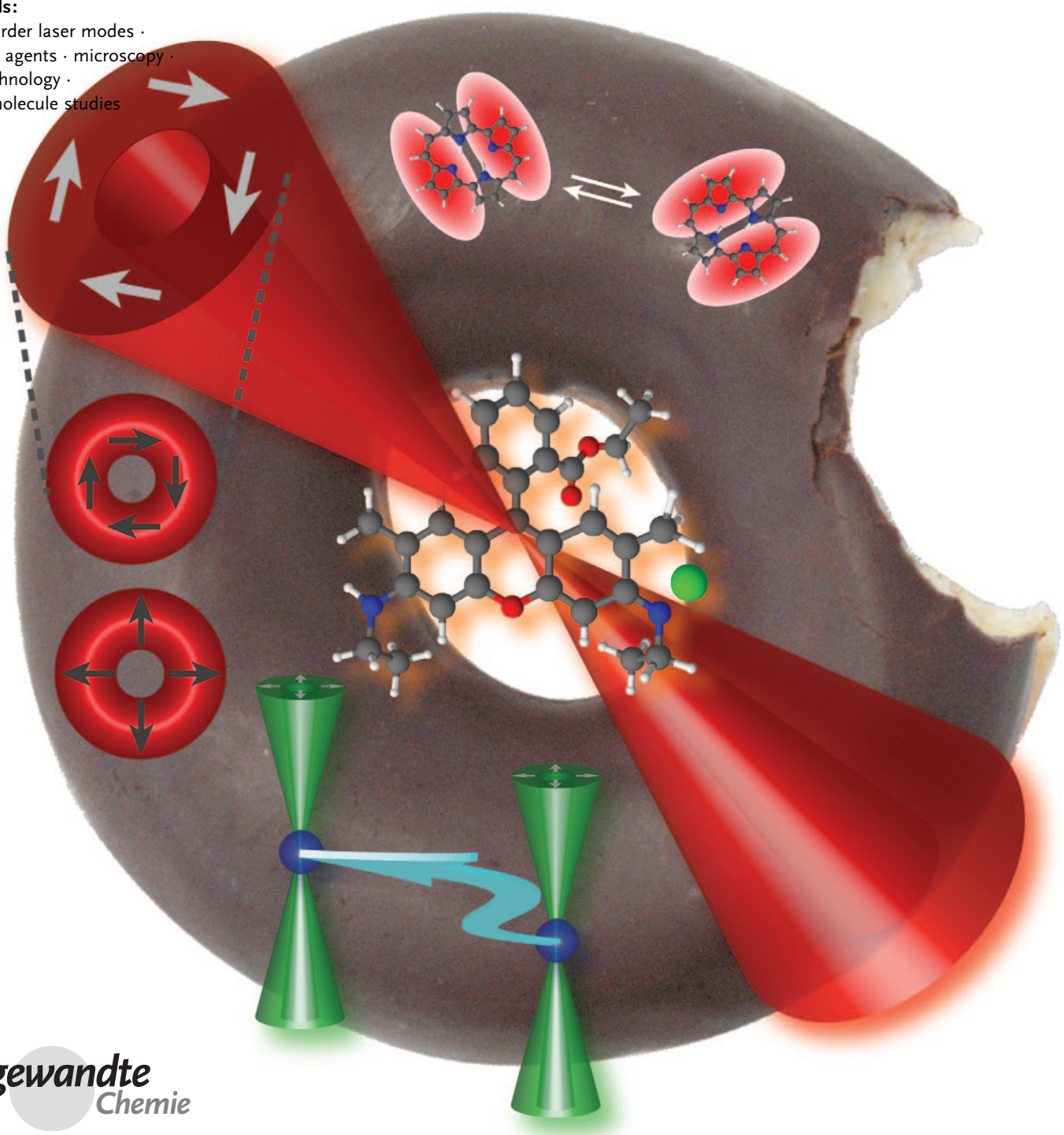

Higher order laser modes, mainly called doughnut modes (DMs) have use in many different branches of research, such as, bio-imaging, material science, single-molecule microscopy, and spectroscopy. The main reason of their increasing importance is that recently, the techniques to generate well-defined DMs have been refined or rediscovered. Although their potential is still not fully utilized, their specifically polarized field distribution gives rise to a wide field of applications. They are contributing to complete our fundamental knowledge of the optical properties of single emitting species, such as molecules, nanoparticles, or quantum dots, offering insight into the three-dimensional dipole or particle orientation in space. The perfect zero intensity in the focus center qualifies some DMs for stimulated emission depletion (STED) microscopy. For the same reason, they have been suggested for trapping and tweezing applications.

From the Contents

1. Introduction

Single-molecule microscopy and spectroscopy has become a strong branch of research in many fields of science. Together with other cutting-edge techniques for the detection of single nanoparticles, quantum dots, or cell compartments, as well as the study of their mutual interactions, it forms the basis of a broad interdisciplinary branch of research: nanotechnology.

Innovative techniques, such as stimulated emission depletion (STED)[1] microscopy, photoactivatable localization microscopy (PALM), and stochastic optical reconstruction microscopy (STORM),[2] as well as near-field scanning optical microscopy (NSOM)[3] nowadays allow an optical resolution far beyond the diffraction limit to be reached. These optical approaches are necessary tools of investigation because they permit high resolution 3D microscopy on biological samples or, in the case of NSOM, high resolution comes with the possibility to acquire additional structural information not accessible by high-resolution non-optical techniques. For example, NSOM can simultaneously provide high-resolution images and the Raman spectrum of the specimen while the latter information cannot be obtained by for example, atomic force microscopy (AFM).[4] Although these techniques are and will be extremely important and useful, in some cases, sub-diffraction resolution information can be extracted with a diffraction-limited technique. As an example, different methods have been developed to determine the dipolar orientation of single molecules. In many cases, this involves the manipulation or determination of the polarization of light. Mainly linearly polarized light has been of interest. However, it was demonstrated that more complex states of polarization, such as radial and azimuthal polarization, are more favorable.

In this Review, we concentrate on a special family of higher order laser modes with a typical doughnut-shaped intensity profile, that is, doughnut modes (DMs) with for example, linear, azimuthal, or radial polarization. In recent years, DMs with different polarization properties have been studied in detail both theoretically and experimentally. We first show that many different techniques have been developed to generate such modes with high quality. In addition, a short summary of their physical and optical properties with special emphasis on their characteristics for tight focusing is presented.

Secondly, we describe how their field distribution has been utilized to decrease the size of both a diffraction-limited spot in standard microscopy[5] and a subdiffraction-limited one in STED microscopy.[1] Afterwards, we demonstrate that

[*] T. Züchner, Dr. A. V. Failla, Prof. Dr. A. J. Meixner
Institut für Physikalische und Theoretische Chemie, Eberhard Karls Universität Tübingen
Auf der Morgenstelle 18, 72076 Tübingen (Germany)
Fax: (+49) 7071-5490
E-mail: alfred.meixner@uni-tuebingen.de
Dr. A. V. Failla
Max-Planck-Institut für Entwicklungsbiologie, Tübingen
Spemannstrasse 35, 72076 Tübingen (Germany)

the combination of DMs and confocal microscopy provides a very powerful and versatile tool for single-molecule microscopy and spectroscopy, allowing for extraordinary precision and additional information, such as the molecular orientation[6] or to follow the tautomerization of a single molecule.[7] To emphasize the imaging power of DMs in confocal microscopy, for comparison, we summarize other microscopy techniques which allow the orientation of single molecules to be determined, for example, defocused imaging,[8] polarization sensitive microscopy,[9] and annular illumination.[10]

Continuing our exploration of the imaging potential of DMs and moving over to metal nanoparticles, we show that not only orientational information can be revealed but that, at the same time, also the particle shape can be distinguished.[11] Furthermore, we describe the impact of azimuthally and radially polarized light in several branches of science. For example, DMs contributed relevantly to the characterization of individual silica nanoparticles[12] and to single-molecule studies in optical microresonators.[13] Moreover, because of their favorable properties upon tight focusing, these modes have been used in optical trapping and tweezing experiments.[14] We give a summary of recent successful experiments using particles which could not be trapped by using the traditional Gaussian beams.[14b–e,15] Furthermore, the contributions of DMs to nanotechnology fields, to material sciences, surface optics, near-field optics, second harmonic generation (SHG), and two-photon microscopy could not be neglected in this Review. For example, we mention the application of radially polarized light in tip-enhanced near-field optical microscopy (TENOM) and present interesting findings achieved by combining radially polarized light with surface plasmon resonance (SPR) imaging[16] as well as in SHG microscopy.[17] Finally, we show how DMs can be applied in industrial applications, that is, to improve the cutting or drilling of metals with focused laser beams.[18]

Although, as it is shown in this Review, the applications of DMs are still somewhat scattered, they provide links between many different fields of science ranging from pure optics and theoretical optics to biomedical applications or the cutting of metals. In recent years, there has been a vivid development in the generation techniques involving DMs. Similarly, the proceeding implementation in microscopy will certainly lead to a true avalanche of fascinating applications. We are confident that the favorable properties of these modes provide a versatile tool to open a new gateway to the nanoworld.

2. Synthesis of Doughnut Modes and Their Optical Properties

2.1. Formal Description of a Doughnut Mode

In this Section, a short and simple theoretical description of a doughnut mode (DM) is provided. The main purpose is to give a clear idea about what DMs are and where their name comes from. As mentioned before, DMs have been used by scientists working in completely different fields, therefore the definitions and acronyms might not always comply with the ones given in some of the literature. These differences, however, are not conceptual but only formal.

These modes and any linear combination of them can be resonant in a laser cavity, thus they are called higher order laser modes (HOLMs).

However, HOLMs also propagate outside a laser cavity, that is, they can be called laser beams. Such beams can be generated with a ring shape: with a circular intensity profile and a dark central zone. Therefore, these beams are called doughnut modes (DMs),[5a,11a,18b,19] doughnut beams (DBs),[13a,18b,20] HOLMs,[21] and also (cylindrical or optical) vector beams.[22] In the following, for the sake of simplicity, we will call them DMs.

DMs are electromagnetic fields and like all electromagnetic fields they must obey the Maxwell equations. In particular, the spatial expression of any electromagnetic field propagating in a homogeneous medium away from any field source, such as electrical charges or currents, must be a solution of the Helmholtz equations [Eq. (1)]

$$\begin{aligned}\left(\frac{\partial^2}{d^2x}+K^2\right)E(x,y,z)=0\\ \left(\frac{\partial^2}{d^2y}+K^2\right)E(x,y,z)=0\\ \left(\frac{\partial^2}{d^2z}+K^2\right)E(x,y,z)=0\end{aligned} \tag{1}$$

where E is the electric field and K the wavenumber.

The solution E_g of the Helmholtz equations represents the more common spatial field distribution generated in a laser cavity [Eq. (2)]

$$E_g(x,y,z)=E_0\frac{w_0}{w(z)}\ \exp\left(-\frac{x^2+y^2}{w(z)^2}\right)\ \exp\left[i\left(kz-\eta(z)+\frac{k(x^2+y^2)}{2R(z)}\right)\right] \tag{2}$$

Tina Züchner studied Chemistry at the Eberhard Karls University, Tübingen and graduated in 2006. Currently, she is working on advanced light-microscopy techniques with individual gold nanoparticles in the group of Prof. A. J. Meixner. Her experiments mainly involve azimuthally and radially polarized light.

Antonio Virgilio Failla studied physics at the University of Rome la Sapienza where he graduated in 2000. He obtained his PhD in 2002 from the University of Heidelberg. Currently, he directs the light-microscopy facility at the Max Plank Institute for Developmental Biology, Tübingen where he develops advanced light-microscopy techniques focusing on their application in bio-imaging.

where $w(z) = w_0\sqrt{1+\frac{z^2}{z_0^2}}$ is the beam waist, $R(z) = z\left(1+\frac{z_0^2}{z^2}\right)$ is the beam radius and $\eta(z) = \arctan\frac{z}{z_0}$ is the phase correction and E_0 the field amplitude at $z = z_0$.

This solution is called the Gaussian mode, because of its profile, or the fundamental mode because from its spatial derivative, two independent families of solutions can be obtained, the Hermite–Gauss (HG) modes E_{mn}^{HG} [Eq. (3)]

$$E_{mn}^{HG}(x,y,z) = w_0^{n+m}\frac{\partial^n}{dx^n}\frac{\partial^m}{dx^m}E_g(x,y,z) \tag{3}$$

and the Laguerre–Gauss (LG) modes E_{mn}^{LG} [Eq. (4)].

$$E_{mn}^{LG}(x,y,z) = k^n w_0^{m+2n} e^{ikz}\frac{\partial^n}{dz^n}\left(\frac{\partial}{dx}+i\frac{\partial}{dy}\right)^m\left[E_g(x,y,z)e^{-ikz}\right] \tag{4}$$

DMs can be generally expressed as a linear combination of HG or LG modes [Eq. (5)].

$$E_{DM} = E_{10}^{HG} + E_{01}^{HG} = E_{01}^{LG} \tag{5}$$

They can have all the conventional states of polarization, for example, linear, circular, or elliptic, however, because of their doughnut shape, they can be in more complex states of polarization as radial and azimuthal polarization. The polarization vectors of the radially polarized DM (RPDM) are aligned like the spokes of a wheel. In the case of the azimuthally polarized DM (APDM), the vectors follow the rim of the wheel (see Figure 1, right). Providing different polarization directions makes these DMs especially appealing for microscopic applications as will be shown throughout this Review.

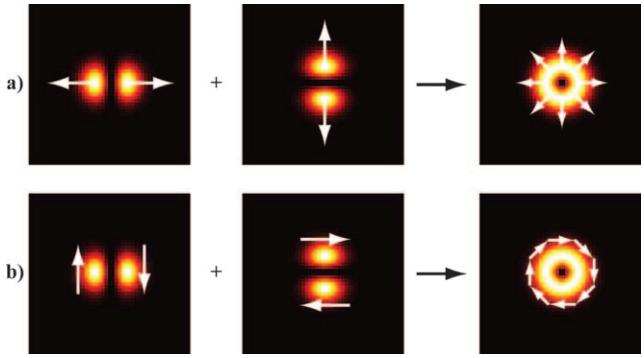

Figure 1. Generation of a a) radially polarized doughnut mode (RPDM) $E_{RPDM} = E_{10}^{HG}n_x + E_{01}^{HG}n_y$ and b) of an azimuthally polarized doughnut mode (APDM) $E_{APDM} = -E_{10}^{HG}n_y + E_{01}^{HG}n_x$ from two appropriate Hermite–Gauss (HG) modes. The radial and azimuthal polarization distribution is indicated on the right.

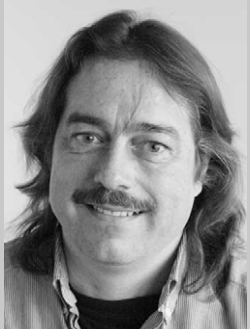

Alfred J. Meixner received his diploma in chemistry in 1984 and his PhD in 1988 from the Swiss Federal Institute of Technology (ETH) Zurich. He earned his habilitation in physics from the University of Basel and is currently full professor of physical chemistry and director of the Institute of Physical and Theoretical Chemistry at the Eberhard Karls University, Tübingen. His current research interests are optical single-molecule spectroscopy and near-field optical microscopy.

The field of a RPDM or APDM (E_{RPDM}/E_{APDM}) can also be expressed in terms of HG modes [Eq. (6)]

$$\begin{aligned} E_{RPDM} &= E_{10}^{HG}n_x + E_{01}^{HG}n_y \\ E_{APDM} &= -E_{10}^{HG}n_y + E_{01}^{HG}n_x \end{aligned} \tag{6}$$

where $n_{x,y}$ are the polarization vectors along the x and y axis.

In Figure 1, the representations of the RPDM/APDM intensity distribution are shown, these result from the sum of the appropriate first-order HG modes.

2.2. Generation of a Doughnut Mode: The Mode Conversion

Doughnut modes are generated by adding up first-order HG modes (see Figure 1). These modes can oscillate in a laser cavity. Thus, it is possible to realize a DM directly in a laser cavity.[23] Particular attention was paid to generating RPDMs and APDMs in the laser cavity.[10a,23d,24] For the sake of experimental flexibility, so that in experiments DMs can be used together with normal Gaussian beams, different methods were developed to produce DMs outside the laser cavity. The optical device that produces DMs is called mode converter (MC) because it converts the Gaussian or the first-order HG mode passing through its input into a DM. Often, the MC not only gives rise to a DM but also determines its state of polarization. In the last 20 years, several kinds of MCs were designed.

In Figures 2 a–g several different types of MCs are schematically described. In Figure 2 a the MC that generates linearly polarized DMs is shown. It consists simply of a circular on-axis beam stop that removes the central part from a collimated Gaussian beam before entering the microscope objective.[10a] Alternatively, an optical phase plate consisting of a planar glass substrate with a thin layer of MgF_2, evaporated on a central circular area can be used.[25] This layer, producing a $\lambda/2$ delay, reverts the sign of the wave amplitude with respect to the remaining ring-shaped area.

RPDMs or APDMs can, for example, be obtained interferometrically, as shown in Figure 2 b. In one of the arms, the polarization is turned by 90° and a proper phase shift is added before recombination. High quality monochromatic beams are thus produced while a Fabri–Perot (FP) interferometer is often used for mode cleaning. The technique is suitable to convert a HG_{01} mode[26] as well as a circularly[26] or linearly[27] polarized Gaussian mode into a RPDM. Note that an APDM can be turned into a RPDM (and vice versa).[18a] Also a linearly polarized DM can be produced interferometrically.[28]

Different kinds of multi-sector retardation plates are able to transform a linearly polarized Gaussian beam in a DM of different polarizations, for example, radially and azimuthally polarized, as sketched in Figure 2 c. The incoming linear polarization passes through an anisotropic retardation plate which locally rotates the polarization. Turning the multi-

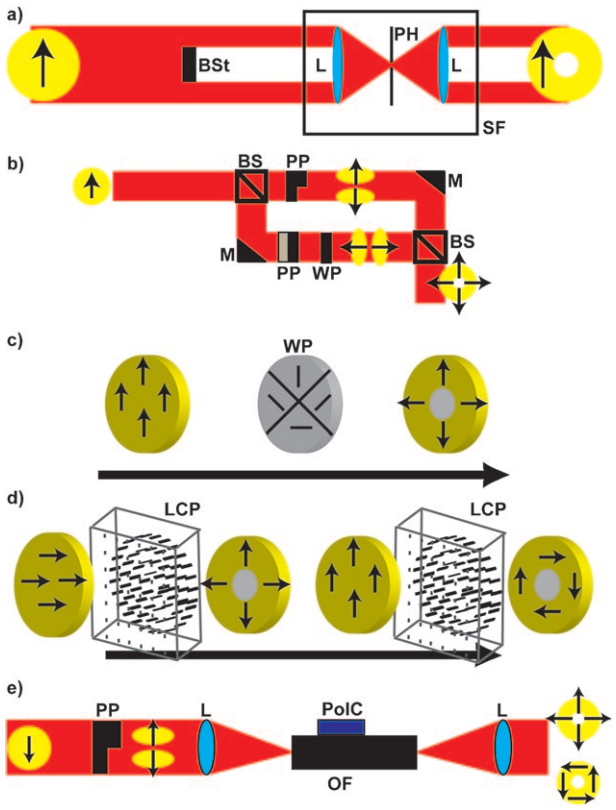

Figure 2. Schematic representations of five different mode converters (MCs): a) For generating a linearly polarized doughnut mode, a beam stop (BSt) is used to block the central part of a linearly polarized Gaussian beam; the beam is directed into a spatial filter (SF) to clean up distortions. The SF is formed by a pinhole (PH) placed in between two lenses (L). b) Interferometric setup for generating a RPDM. A linearly polarized Gaussian beam is equally divided by a beam splitter (BS) before entering the two arms of an interferometer. In each arm, the Gaussian beam is converted into a first-order HG mode by passing through a phase plate (PP). In one of the two arms, the beam passes through a lambda half wave plate (WP) to turn the polarization by 90°. Finally, the beams are recombined by a second BS giving rise to a RPDM. Note that the light is properly directed into the MC by a series of mirrors (M). c) An opportunely oriented four-quadrant lambda half wave plate (WP) can convert a Gaussian beam into a RPDM. Note that rotating the same WP by 90°, an APDM can be produced (not shown). d) A liquid-crystal plate (LCP) exploiting the twisted nematic effect converts a linearly polarized Gaussian beam into either a RPDM or an APDM. The black lines represent the orientation of the LC domains. e) Generation of RPDMs or APDMs with a multimode optical fiber (OF). A linearly polarized Gaussian beam is converted into a first-order HG mode and focused by a lens (L) into the OF. The polarization converter (PolC), a device that twists and presses the OF, is used to generate either a RPDM or an APDM at the OF output. The output beam is finally collimated by another lens. Note that the OF can be used to generate more than one RPDM/APDM simultaneously at different wavelengths.

sector retardation plate by 90° allows the output to be switched between a RPDM and an APDM. The simplest of these MCs consists in a four-quadrant $\lambda/2$ wave plate.[5b,19b] Other similar systems employ, for example, segmented photonic crystal $\lambda/2$ wave-plate MCs,[29] eight-sector $\lambda/2$ MCs,[30] or spiral retardation plate MCs.[31] The beam quality can be improved by inserting either a FP interferometer or a spatial filter.[11a] All the MCs discussed above are more or less monochromatic, that is, for each wavelength a different retardation plate has to be used.

To circumvent this problem, that is, to allow one MC to work with different wavelengths or to produce a polychromatic DM, liquid-crystal (LC) cells or optical fibers (OFs) have been employed. LCMCs can be tuned to different wavelengths. A LCMC can be a double-layer LC cell. In one layer, the LC molecules are all oriented along a given direction while in the second layer the molecules are differently oriented along segments that together form a circle.[32] A schematic diagram of a LCMC is given in Figure 2d. A LCMC can use the twisted nematic effect[33] in combination with the $\lambda/2$ wave-plate effect in LC devices that have spatially variable alignment layers. We can consider the LCMC as a particular spatial light modulator (SLM). It is important to mention that this kind of MC, and in general SLMs, are commercially available. LC panels have also been used to produce hologram-based MCs[34] extending a previously developed technique that allows complex fields to be produced with different geometries.[35]

Potentially more interesting for the generation of wavelength-tunable or multicolor DMs in a commercial microscope are the multimode optical-fiber MCs.[22b,24f,36] A variety of differently polarized modes are freely propagating in a multimode fiber. The MC strategy can be summarized in two steps. In the first one, the number of modes propagating in the fiber is limited by choosing a proper cut off and by coupling the beam into the fiber in a corresponding way, for example, by focusing a beam after passing through a two-sector $\lambda/2$ retardation plate. The second step consists of selecting the desired mode by, for example, twisting and pressing the fiber at a given point.[36b,c] Such a MC is schematically represented in Figure 2e. Naturally, herein it is not possible to classify all the MCs designed to produce a DM; for more details, see for example, Reference [37].

2.3. Focusing Doughnut Modes of Different Polarizations

The experimental implementation of DMs is an easy and straightforward step. As a practical example for combining the production and utilization of DMs, a standard confocal setup is shown in Figure 3a. Both the fluorescence and reflection path are shown schematically. Note that the mode converter (MC) is the only element needed to couple DMs into a standard confocal setup. Several MCs take up only a little space, especially those based on liquid crystals (LCs) and the ones with multi-sector retardation plates. However, the use of DMs also requires the knowledge of their optical properties in the focus of a high numerical aperture (NA) lens. Hence, the study of the electromagnetic fields produced by focusing DMs with a high NA lens has involved both theoretical and experimental (e.g. Refs. [5a,22a,23c,38]) investigations. In continuing progression, experimental and theoretical studies are following each other, alternately

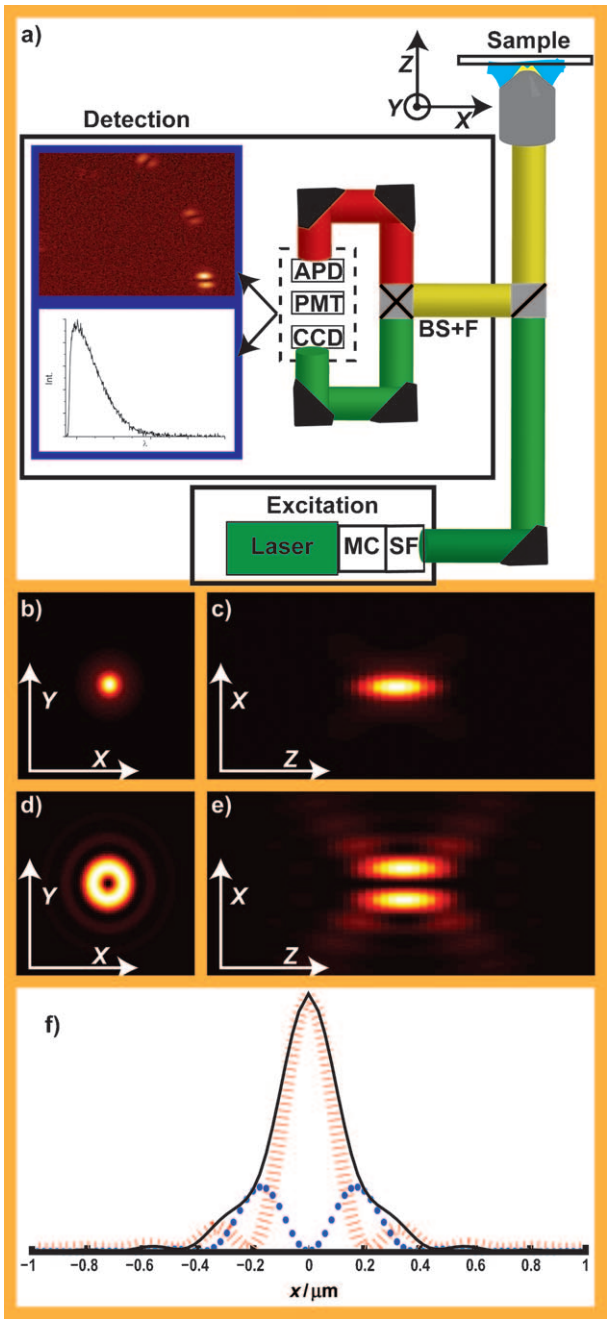

Figure 3. a) Schematic representation of a confocal microscope setup: the light generated by a laser passes through a mode converter (MC) and a spatial filter (SF) and is directed to the sample. All the signal coming from the sample is sent to the detection path by a beam splitter (BS). The combination of a BS and an appropriately chosen band pass filter (F) allows the user to split the elastically scattered light (green beam) from the fluorescence/luminescence and not elastically scattered light (red beam). Finally, the signal of the sample allows spectra or optical images to be acquired using any combination of a charged coupled device (CCD), avalanche photo diode (APD), and photo multiplier tube (PMT) detectors. b),d) *XY* focal projection of the calculated intensity distribution of a RPDM and an APDM respectively, the image size is in both cases $2\times2\ \mu m^2$. c),e) *ZX* focal projection of the calculated intensity distribution of a RPDM and an APDM, respectively, the image size is in both cases $4.5\times2\ \mu m^2$. f) Normalized cross sections of the intensity distribution of a RPDM with the total intensity (black continuous line), the longitudinally polarized component (red dashed line) and the transversally polarized component (blue dotted line). The simulations shown were performed with a fixed $NA = 1.4$ in all cases.

inspiring both sides for more detailed theoretical[22d,39] and sophisticated experimental[22c,40] work.

The general approach for calculating the field distribution near the focal point of a collimated beam focused by an aplanatic lens is described in Ref. [41]. Richards and Wolf started from the generic result[42] that the electric (and also the magnetic) field distribution of a collimated beam focused by a generic aplanatic lens can be described as the weighted integral sum of plane waves converging to the focus region from a given angle. A detailed description of these calculations is beyond the purpose of this Review and can be found, for example, in Refs. [41,42]. The particular case of focusing DMs by a high *NA* objective can be also found in the literature.[16a,19a,22] The numerical results presented regarding the focusing of RPDMs and APDMs were obtained following critically the theory described in Ref. [19a].

In Figure 3b–e, the calculated intensity profiles of both a RPDM and an APDM focused by a high *NA* objective ($NA = 1.4$) are shown. Note that RPDMs focused by high *NA* lenses change their intensity distribution in the focal plane, passing from the classical doughnut-shaped intensity distribution (see Figure 1a) to the "Gaussian-like", as shown in Figure 3b. Such a profile is sharper than the one obtained with a conventional Gaussian beam, leading to a small gain in the optical resolution (see Figure 3f and Section 3).[5a–c] The shape transformation is due to the splitting in two polarization components: a dominant longitudinal and a weaker lateral one. The first is polarized along the optical axis (longitudinal component) while the second is polarized in the image plane (lateral component). The relative intensity of the two is strongly influenced by the *NA* of the focusing lens. The higher the *NA*, the stronger the longitudinal component becomes. Another parameter is the size of the dark central zone of the DM before focusing which can be influenced for example, with a circular beam stop.

The combination of a large central dark zone together with a high *NA* leads to an especially strong longitudinally polarized field which makes it the right candidate for such applications as apertureless near-field microscopy, where a strong excitation field parallel to the optical axis is desired. At a high *NA*, the lateral component of a RPDM is dominated by the longitudinal one but it is not totally suppressed, thus, a RPDM can also be used to probe 3D structures with a light microscope.

APDMs seem to be less tunable in their shape, and their field distributions do not present any dramatic changes upon focusing. The field of an APDM keeps parallel to the focal plane and the intensity profile always stays ring-like, independently of the lens *NA* or the size of the dark central zone of the collimated beam. APDMs are not as powerful as RPDMs for imaging 3D structures because of the lack of a longitudinal component. But they are perfectly suited to study processes which occur at special planar interfaces, such as, the interface between two dielectric media.[43]

3. Improving the Optical Resolution in Light Microscopy with Doughnut Modes

Light microscopy and spectroscopy are unique tools to image and to study the physical, chemical, and biological properties of a specimen. Moreover, it is one of the least invasive imaging techniques and the only one suitable for live imaging. Despite all these advantages, light microscopy results have less resolution than, for example, atomic force microscopy (AFM) or electron microscopy (EM). Therefore, different approaches have been carried out to increase the optical resolution in light microscopy involving DMs.

In light microscopy, the optical resolution is partly given by the size of the excitation beam in focus, that is, the excitation point spread function (PSF). The essential impact of the detection part on the resolution is beyond the scope of this Review and is therefore omitted. The size $\delta_{x,y,z}$ of the focal spot generated by the Gaussian beam for a high NA lens is diffraction limited as described by Abbe's law [Eq. (7)]

$$\delta_x, \delta_y = \frac{\lambda}{2NA}; \delta_z = \frac{2n\lambda}{NA^2} \tag{7}$$

where λ is the wavelength of the excitation beam, NA is the numerical aperture of the focusing lens and n is the refractive index of the surrounding medium. The terms $\delta_{x,y,z}$ are proportional to the full-width at half maximum (FWHM) of the beam intensity profiles along the lateral and longitudinal direction which are a direct measure of the optical resolution. For applications involving 3D image stacks, the longitudinal resolution δ_z is of considerable importance. However, for most applications discussed in this Review, the lateral resolution $\delta_{x,y}$ is of main interest. To allow for a wavelength-independent comparison, one alternative is to give the area of the focal spot A in units of the arbitrary factor f of the squared wavelength λ^2 as it is common in some of the optics literature cited herein [Eq. (8)].[5a–c]

$$A = \frac{(\mathrm{FWHM})^2\pi}{4} = f\lambda^2 \tag{8}$$

For better comparison, we will give both values for the FWHM and the area in units of λ^2 in the following. DMs in different states of polarization contribute to increase the lateral resolution in light microscopy. Linearly polarized DMs have been used in stimulated emission depletion (STED) microscopy. This not-diffraction-limited light microscopy technique exploits the physical chemical properties of the dyes (fluorescent proteins) used to label a specimen and can be applied only in point scan (laser scan or raster scan) microscopy. With STED, a resolution of about 20 nm ($8\times10^{-4}\,\lambda^2$ at 633 nm) can be achieved even for biological samples.[44] The technique's principle is described below while further details can be found in the literature.[2,44] First, the excitation beam is turned on and all the dye molecules are transferred into the excited state. Then, a second pulsed beam, the so-called depletion beam is focused on the same spot shortly after the excitation beam. The wavelength of this second beam is chosen such that it produces a field which matches the energy difference between a vibrational level in the excited state and one in the ground state. As a consequence, stimulated emission is induced and the excited state is depopulated. In the detection path, the light emitted at the depletion beam frequency is filtered out and only the fluorescent light is detected. In other words, a nonlinear system has been created that keeps bright (active) a small number of molecules in a limited (small) region of the diffraction-limited focal spot while keeping dark (inactive) all the others.[2]

The intensity, the shape,[45] the pulse frequency, as well as the time duration of the depletion beam are parameters to be considered and adjusted. The shape of the depletion beam is chosen in such a way that it overlaps with the excitation beam everywhere except for a small area in its center. This arrangement means that a linearly polarized DM is a good candidate[45] and indeed it was used as the depletion beam, for example, in Ref. [46]. Increasing the intensity of the depletion beam induces a more efficient depopulation of the excited state through stimulated emission and in the same time reduces the dark central zone of the focused DM. Hence, tuning the intensity of the depletion beam in principle allows the resolution to be adjusted since fluorescence only occurs in the central spot of the DM which can be reduced to sizes of a few nanometers. As long as practical problems such as molecular bleaching induced by the high intensity of the depletion beam and detection sensitivity are not concerned, single-molecule detection with nanometer accuracy is in principle possible. To circumvent the resolution limit also along the optical axis, it was proposed to use a circularly polarized DM as the STED depletion beam[45] or to combine STED and 4pi microscopy.[47,48] In a special case, a RPDM focused by a paraboloid mirror was suggested as a depletion beam since a tight and almost spherical dark central zone can be produced in the focal region.[49] DMs were used similarly in Ref. [50]. In this case, the depletion beam temporarily excites a photoswitchable protein to an energy level which is a non-fluorescent state.[50]

For applications in standard light microscopy, radially polarized light is of special interest. When a RPDM is focused, the longitudinal component overwhelms the transversal one for a $NA \geq 1$. Therefore, we will consider a high NA to be a value greater than or equal to 1, below this value, we will call it a low NA, although this should not be mistaken as a general definition. Tightly focusing a RPDM with a high NA focusing element generates a smaller focal spot size[5a–c] than can be achieved for linearly polarized light[5a] ($0.311\,\lambda^2$ vs. $0.26\,\lambda^2$ or 400 vs. 360 nm at 633 nm for $NA = 1.0$). The longitudinal component is focused to an even smaller area of $0.16\,\lambda^2$ (290 nm at 633 nm for $NA = 1.0$) as shown both theoretically and experimentally.[5a,b] The highest gain in resolution is achieved with an annular aperture in the back focal plane of the lens ($0.11\,\lambda^2$/210 nm at 633 nm for $NA = 1.0$).[5a,b] Compared to the resolution achievable with conventional illumination, these values correspond to an improvement by a factor of two. With a parabolic mirror as the focusing element (with an extraordinary high $NA = 1$ for an air focusing element), a slightly different field distribution in focus is found. The spot size was shown to measure $0.134\,\lambda^2$ (260 nm at 633 nm).[5c] To our knowledge, this is the smallest

focus ever achieved using an air focusing element. Another benefit of a parabolic mirror is that the longitudinal component is predicted to be approximately 14-times stronger than the transversal one,[6b] while a factor of 2–3 is achieved for a high *NA* microscope objective.[5b,6a] Using a circularly symmetric plasmonic lens as the focusing element has been shown to further increase lateral resolution.[5d,e] Although the experimental values did not yet reach the theoretically predicted limit, the results are very promising.

The tighter focusing of light for radial polarization has recently found some application to improve the lateral resolution in different fields of microscopy. In total internal reflection fluorescence (TIRF) microscopy, only the longitudinal component of the focused field is involved. Therefore, the smaller focal area as well as the increased field strength and the spot-like shape of the RPDM's longitudinal component are of benefit compared to the relatively weak and two-lobed *z*-component of a linearly polarized beam. These advantages have been studied both in theory and experiment for TIRF microscopy.[51] Also in coherent anti-Stokes Raman scattering (CARS), an improved lateral resolution has been found combined with an orientational sensitivity.[52] Thus, a combination of linear and radial polarization should allow the full 3D orientation of molecules to be determined with CARS.[52]

As discussed above, radially polarized light allows the optical resolution to be increased as long as a high *NA* focusing element is used. Paradoxically, Tang et al. showed that this is also possible using a lower *NA* of 0.9.[53] In this case, the PSF of the RPDM in focus is doughnut shaped and even larger than the PSF of a Gaussian beam. Therefore, the optical resolution is smaller for conventional detection. However, Tang et al. implemented a mode conversion into linear polarization in the detection path which allowed the use of a much smaller pinhole. Hence, both the confocality of the system and the lateral resolution increased even over those found for pure linear polarization.[53]

In Sections 5–7, we will summarize some applications of DMs where subresolution information is revealed without breaking or improving the classical diffraction limit.

4. Microscopic Techniques to Determine the Orientation of Single Molecules

In the last decades, single-molecule microscopy and spectroscopy have found wide application in (physical) chemistry, physics, and biology. One important parameter involved is the orientation of the molecular dipole and hence the molecule itself. This knowledge is important, for example, for precise distance measurements or to accurately determine Förster resonance energy transfer (FRET) efficiency. Moreover, the lifetime and emission intensity varies with the molecular orientation, for example, at an interface.[54] For molecules embedded in polymers, changes in their orientation reveal dynamics of the surrounding matrix. The orientation of dye labels can indicate orientational changes in proteins and peptides, thus giving insight into the biological functioning of molecular machines. Naturally, the orientation can only be determined on the single-molecule level, or when an ensemble of molecules is not randomly oriented (opposite transition dipoles will delete each other). Therefore, in most applications, extreme sensitivity is necessary.

In the last few decades, different techniques have been developed to extract the orientation of single dipoles. To emphasize the dramatic improvement that DMs hold for single-molecule microscopy and spectroscopy, a general overview will be given on other orientational methods pointing out their advantages, disadvantages, and limitations. For convenience, we will first summarize the well established techniques, such as defocused imaging and polarization sensitive techniques. The impact of DMs will follow.

To simplify the discussion about the orientation of a dipole moment, an angular description is introduced. In general, two different angles must be discerned when defining the 3D orientation of a nanoobject. One is the in-plane component ϕ, which lies in the sample plane. The second component is the out-of-plane angle θ between the object and the optical axis (Figure 4). In such a way, both the orientation of the absorption dipole moment and of the emission dipole moment of a molecule can be described, both of which can serve as a measure of the molecular orientation. Note that for the absorption of light its polarization direction has to match the orientation of the absorption dipole moment. Similarly, the emitted light is polarized in the direction of the emission dipole orientation.

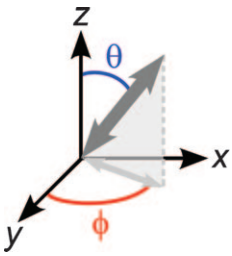

Figure 4. The determination of the 3D orientation of a dipole with the in-plane angle ϕ and the out-of-plane angle θ.

4.1. Defocused Imaging

In many cases acquiring slightly defocused images reveals additional information not directly accessible under tightly focused conditions, regarding, for example, the orientation of single dipoles. Prior to the use in wide-field microscopy, the concept has been used with mirror objectives and in TIRF microscopy. A general drawback of defocused techniques, however, is the reduced signal-to-noise ratio accompanied by a lower sensitivity. Additionally, defocusing gives larger patterns than focused techniques and consequently, single objects have to be further apart for proper imaging. However, provided that the signal is strong enough, the localization can be even more precise than for focused techniques.[8e,55]

Several defocusing techniques have been developed. In the first one a mirror objective was used to study the orientation of single terrylene molecules at cryogenic temperatures.[8a,b] Orientational information at room temperature was first obtained in TIRF microscopy exploiting slight aberrations introduced by a thin water layer on the sample. Thus, the 3D molecular orientation could be determined with a high accuracy of 1–2° on a 100 millisecond timescale.[8c,d] Further development of the technique resulted in the

combination of focused and slightly defocused imaging to extract the 3D orientation.[8e]

In a biological application of defocused TIRF microscopy, ligand–protein interactions have been studied with video rate imaging.[56] In addition, the technique seems to be highly sensitive because the luminescence from single ions could be detected.[57]

The presented concept of defocusing has been used later in epifluorescence microscopy.[8f,g] In 2D, the acquired two-lobed patterns directly visualize the dipolar orientation. An experimental defocused wide-field image of single Cy5 molecules is shown in Figure 5, accompanied by the fitted

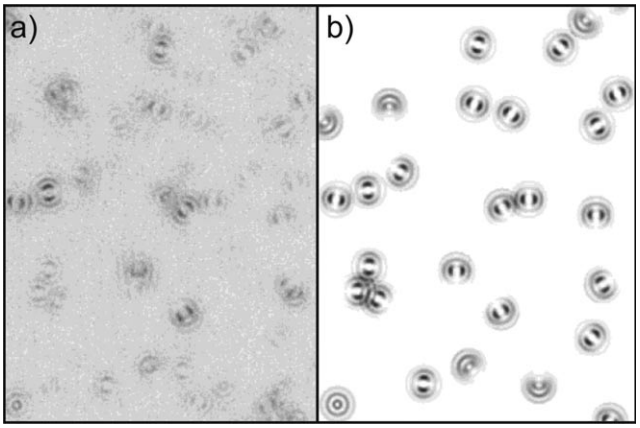

Figure 5. Sections of wide-field defocused (1 μm) epifluorescence images of single Cy5 molecules. a) Experimental image, b) composite calculated image displaying identified molecules and their attributed patterns. The fitting procedure allows the 3D orientation of every molecule to be extracted. Adapted with permission from Ref. [8g]. Copyright 2004 American Chemical Society.

calculated patterns. A drawback of the technique, however, is the relatively poor accuracy of 15° for in-plane angels (ϕ) and of 30° for out-of-plane angles (θ).[8f,g,58] The defocusing also reduces the signal-to-noise ratio and hence the sensitivity.

Defocused wide-field imaging helped to reveal the stepping behavior of myosin V as it moves along actin.[59a] Many other cases of orientational studies at the single-molecule level using defocused wide-field imaging are in the literature.[58,59]

4.2. Polarization Resolved Techniques

The interaction of light and single molecules depends on the relative orientation of the excitation polarization and the molecular dipole. Measuring the polarization direction of the excitation light and/or the emitted light allows the orientation of the absorption and/or emission dipole moment to be determined. Different schemes have been developed for this purpose and found wide application in different fields of science.

The first observation of single molecules under ambient conditions was realized with near-field scanning optical microscopy (NSOM).[9a] Fitting the experimental patterns with theoretically predicted ones[9a] allowed the 2D orientation to be determined with an accuracy of a few degrees, combined with the high localization precision of 1 nm, all on a timescale of 10^{-2}–10^{3} s.[9b]

Measuring the orientation of the absorption dipole moment by modulating the excitation polarization has been widely used to determine the orientation of single molecules. The work ranges from orientational studies in matrices at 1.8 K[9c] or with the very high accuracy of 0.2°[9d] to moving proteins.[60] Weston and Goldner developed a variation of the technique in which the orientation is color-coded in the resulting images. Hence, rotating molecules change their color (see Figure 6).[9e]

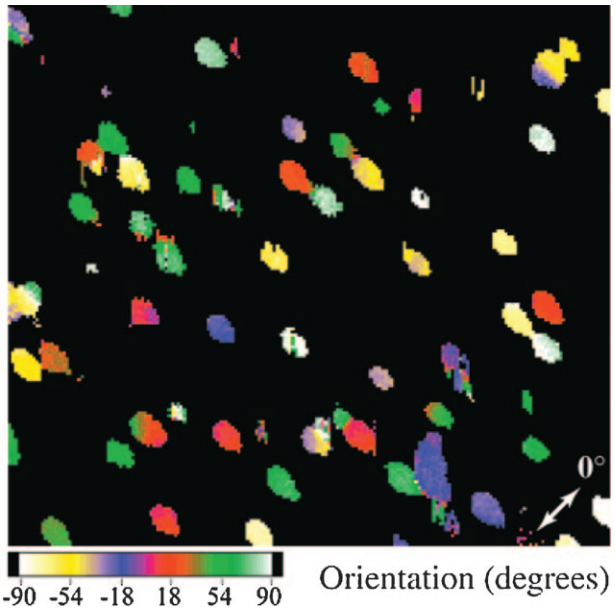

Figure 6. Orientation image of single $DiIC_{18}$ molecules in a thin PVB film (image length 20 μm). The orientation was deduced from the phase of the modulated fluorescence, regions with fluorescence signal below 7 kHz have been excluded from the color scale (appear black) for better visualization. Note that rotating molecules show more than one color. Reprinted in part, with permission from Ref. [9e]. Copyright 2001 American Chemical Society.

To extract the full 3D orientation, modulating the excitation polarization has been combined with TIRF microscopy. One drawback, however, is the lack of resolution for dipoles being close to perfect in- or out-of-plane orientation ($\theta \approx 0, 90°$).[9f]

The orientation of the emission dipole moment can also be used to monitor the rotation of single molecules. In most cases, two detectors are used which are sensitive to perpendicular polarization orientations (x and y). The intensity ratio of the two detectors depends on the dipolar orientation and can thus be extracted [Eq. (9)][9b,g,61]

$$\phi = \tan^{-1}\sqrt{\frac{I_x}{I_y}} \qquad (9)$$

while the intensities I_x, I_y measured on the two channels might to be corrected with a weighing factor accounting for different detection efficiencies. The values for the orientation of the emission dipole range from 0 to 90° [see Eq. (9), with an "uncertainty" of $n\pi$]. Linearly polarized light can be used for excitation. To compensate for different absorption efficiencies, circularly polarized light can be used for excitation.

This technique revealed the dipole orientation of DNA–fluorophore complexes as well as their rotation and adsorption dynamics and showed that the absorption and emission dipoles of Cy5 molecules are not perfectly parallel but differ about 5°.[62] Single-molecule rotational studies are also possible on an ultrafast timescale to reveal matrix or molecular dynamics[9g,63] or for use in biological applications.[64] For special, highly symmetric cases, even the 3D orientation can be determined as has been shown for CdSe quantum dots (QDs).[65]

For all these schemes, the excitation field has no significant longitudinal component, therefore only the projection of the dipole moment in the sample plane can be measured. In addition, the determination of the emission dipole orientation is very limited. Hence, there have been some approaches to detect the full 3D orientation of nanoobjects involving polarization sensitivity. For example, a setup with three detectors being sensitive to different polarizations has been suggested,[66] its limitations theoretically discussed,[67] and an experimental setup realized.[68] In a different approach, excitation with different polarizations was achieved. Thus, the 3D orientation of single absorption dipoles can be determined with three successive scans and an accuracy better than 10°[69] or—in a similar approach—with an accuracy of 2°.[70]

4.3. Doughnut Modes and Single Molecules

4.3.1. Linearly Polarized Doughnut Modes

The 3D orientation of single molecules can also be determined without being sensitive to polarization in the detection path. Annular illumination with a linearly polarized Gaussian beam allows the absorption dipole orientation to be roughly determined by the shape of the emission pattern. The strength of the electric field components along the three Cartesian axes are comparable under annular illumination while the shape of the field distribution in focus highly varies. The single molecules probe the electric field distribution and thus the emission patterns result as a superposition of the three "pure" intensity distributions (see the three corners in Figure 7).[10a] Thus, in principle, the orientation can be determined looking at a single fluorescence pattern (see Figure 7), but unfortunately, the technique does not offer high accuracy.[10] A precision around 5° accompanied by a higher uncertainty close to perfect in- or out-of-plane orientations ($\theta = 0$, 90°) has been reported.[71]

In addition, the orientation provided by the fitting procedure slightly differs from the true orientation angle and never results in perfect in- or out-of-plane angles (i.e. $\beta = \theta = 0$, 90°). However, the technique allowed it to be shown again that the fluorescence lifetime of single molecules at an interface strongly depends on their orientation.[54] Besides, the absorption dipole orientation of single FRET pairs is not always collinear even if expected from the molecular structure of the coupled system because the environment might influence the dipolar orientation. Slightly varying the technique, a higher accuracy of 1–2° was achieved by directly imaging the emission patterns in the back focal plane of a high *NA* objective.[10b] However, in our opinion, this sacrifices the intuitive approach of standard imaging techniques.

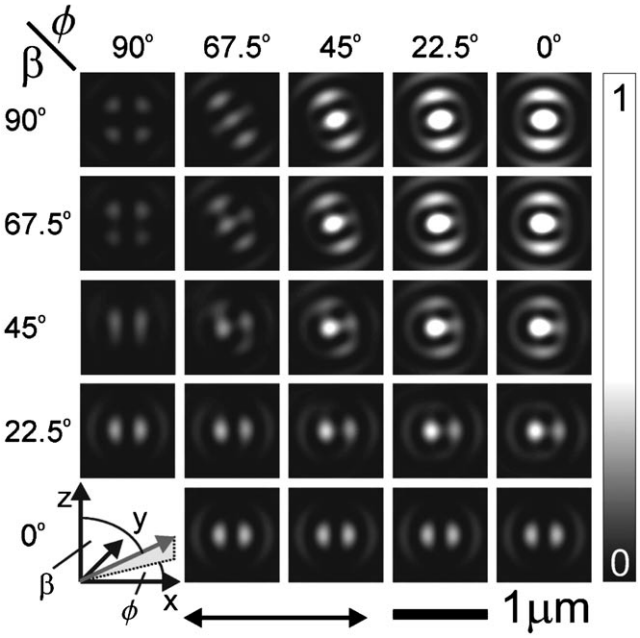

Figure 7. Single-molecule fluorescence patterns 5 nm below the interface calculated from the field distribution. Coordinate system: definition of the dipole orientation angles β and ϕ with respect to the excitation polarization (double arrow). Reprinted with permission from Ref. [10a], Copyright 2000 by the American Physical Society. http://link.aps.org/abstract/PRL/v85/p4482.

The orientation of molecules can also be determined directly with a linearly polarized DM, as has been shown both in theory and experiment.[72] However, the technique is mainly sensitive to dipoles oriented along the optical axis and perpendicular to the direction of polarization. Hence, the orientation of randomly oriented molecules can only be precisely determined for a subpopulation. The theoretical results show that the molecular orientation also influences the gain in resolution for STED microscopy[72a] which coincides with experimental findings.[72b] When both the excitation and depletion beam are linearly polarized, a dramatic effect is found. A better resolution is only achieved for dipoles oriented along the direction of polarization while the resolution is in fact decreased for other orientations. For the experimentally more relevant case of circularly polarized light, the resolution still depends on the orientation.[72a]

4.3.2. Radially and Azimuthally Polarized Doughnut Modes

A very elegant approach to determine the molecular orientation involves the use of radially or azimuthally

polarized DMs, which were introduced at the beginning of this Review. As mentioned above, the interaction of light and single molecules depends on the orientation of the polarization and the dipole moment. The special polarization properties of the DMs offer different orientations of the polarization in focus. As a consequence, the orientation of single dipoles can be directly imaged, knowing the electric field distribution in focus. The pure 2D polarization of the APDM allows the projection of the dipole moment in the sample plane to be imaged. The combination of both a longitudinal and a transversal component as provided by a RPDM allows the full 3D orientation of single dipoles to be determined and thus single molecules.[6]

This feature has been studied theoretically by Lieb et al. for a parabolic mirror[6b] while Novotny et al. examined the same problem for a high *NA* objective, both in theory and experiment.[6a] The longitudinal field of a RPDM can be probed with single molecules.[6a] Vice versa, fluorescence patterns acquired with a RPDM allow the 3D orientation of single dipoles to be determined (see Figure 8).[6a] For a lateral orientation, only the transversal field of the RPDM excites the molecules and a two-lobed pattern is generated which indicates the dipole orientation (connecting the two lobes).[6a] These patterns are reminiscent of those found in defocused imaging (cf. Figure 5). A pure longitudinal orientation leads to a single spot while orientations combining lateral and longitudinal components give patterns in between these two extremes.[6a] A nice agreement between experimental and theoretical predictions has been achieved (see Figure 8).[6a] Moreover, slightly different patterns are expected when a parabolic mirror is used as the focusing and collecting element (see Figure 8 B).[6b]

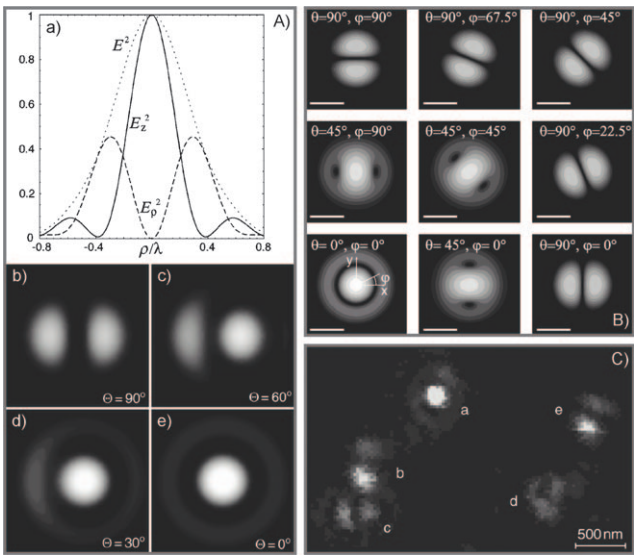

Figure 8. A) a) Comparison of longitudinal field strength E_z^2, transverse field strength E_p^2, and total field strength E^2 as a function of radial coordinate upon focusing with a high *NA* microscope objective (*NA* = 1.4), evaluated 2 nm beneath the interface. b)–e) Calculated emission rate images [*R*(*x*,*y*)] for different polar orientations of a molecule in the *xz* plane. θ denotes the angle between the dipole axis and the beam axis. B) Calculated confocal images, $|E|^2$, of a dipole emitter for different orientations and excitation with a RPDM upon focusing with a parabolic mirror (*NA* = 1.515). The illuminated aperture is reduced to 1.21 and the dipole is scanned in the *xy* plane. The dipole orientation angles as well as the axis are shown in the lower left image. A logarithmic scale is used with a factor of 2 between adjacent contour levels. The scale bar length is one wavelength λ/n. C) Fluorescence rate images [*R*(*x*,*y*)] of arbitrarily oriented molecules excited with a focused RPDM. The dipole moment of molecule *a* is nearly longitudinal (cf. A,d), whereas the dipole moments of molecules *c* and *d* are transverse (cf. A,b). Molecules *b* and *e* have an orientation of $\theta \approx 60°$ (cf. A,c). A),C): Reprinted with permission from Ref. [6a], Copyright 2001 by the American Physical Society. http://link.aps.org/abstract/PRL/v86/p5251. B): Reprinted in part, with permission from Ref. [6b].

Although these results were obtained with a diffraction-limited technique, information from the nanoscale as for example, the orientation of single molecules is directly visible to the naked eye without any data analysis process. Even breaking the diffraction limit[72b] does not reveal this information. Moreover, DMs in special cases allow chemical reactions to be followed on the single-molecule level. For example, the tautomerization of single porphycene molecules has been imaged with azimuthally polarized light.[7a,b] Tautomerism in porphycenes involves the transfer of two hydrogen atoms between the four nitrogen atoms in the inner ring of the molecule. The transition dipole moment of the two chemically identical *trans* isomers had already been shown to differ by 70–80°.[73] Since the tautomerization is much faster than the timescale of the imaging technique, two almost perpendicular dipoles should be observed for each molecule leading to a ring-shaped pattern. Indeed, experimental patterns with almost perfect doughnut shape have been observed (Figure 9 a).[7a,b] In contrast, some of the observed molecules give two-lobed patterns. Combining azimuthal and radial polarization, these patterns could be shown to correspond to molecules standing on their edges or on their vertices (Figure 9 b,c).[7c]

5. Doughnut Modes and Single Metal Nanoparticles

Noble-metal nanoparticles are of increasing scientific interest for microscopic studies. Compared to single molecules and single quantum dots (QDs), the emission from single noble-metal nanoparticles does not bleach. In addition to this stable light emission, the particles strongly scatter the light, thus enabling the detection of single particles. Instead of the dipole moment known from single molecules, the polarizability tensor of the metal nanoparticles comes into play. We showed that combining confocal interference scattering microscopy (CISM) with DMs (APDM and RPDM) allows the orientation of metal nanorods to be determined precisely at dielectric interfaces and to monitor their rotation.[11a,21b,74] Moreover, CISM–DM offers a simple tool to distinguish differently shaped particles by their scattering patterns (Figure 10).[11b] Since such information is not accessible with standard microscopy techniques, this Section will address the topic in more detail.

For the described experiments, a homebuilt inverted confocal microscope with an APDM or a RPDM as excitation sources was used. In CISM, the elastically scattered light from

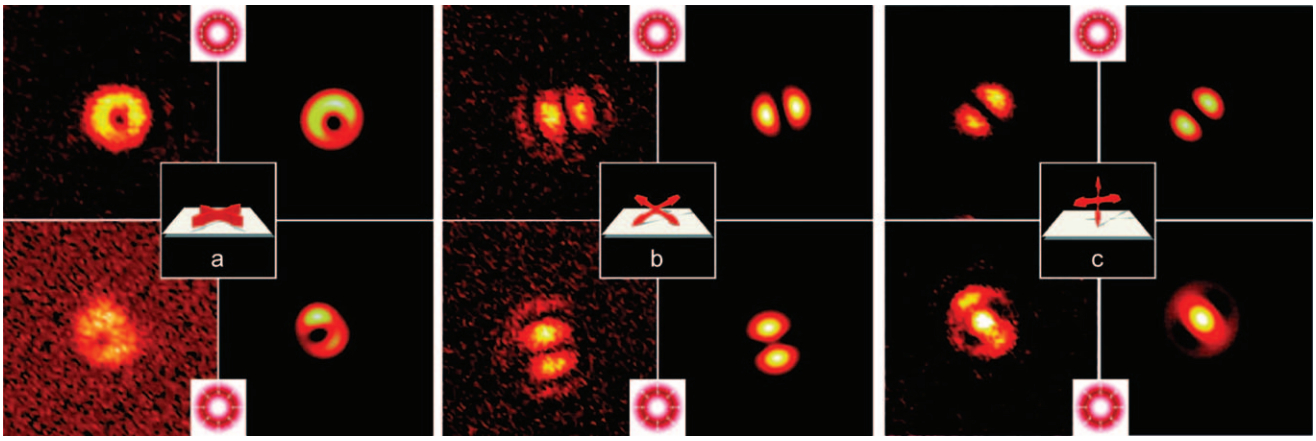

Figure 9. Confocal fluorescence images observed for a porphycene derivate (2,7,12,17-tetra-*tert*-butylporphycene) excited either by an APDM (top) or a RPDM (bottom), showing three different orientations of the chromophore. a) A molecule lying flat on the surface; b),c) molecules with perpendicular orientation of the molecular plane with respect to the sample surface. In (b), two dipoles form the same angle with the surface plane (molecule on the edge), whereas in (c) one dipole is perpendicular to the surface and the other is almost parallel to it (molecule stands on one vertex). Left: experimental pattern; right: simulated pattern. Reprinted with permission from Ref. [7c]. Copyright 2009 American Chemical Society.

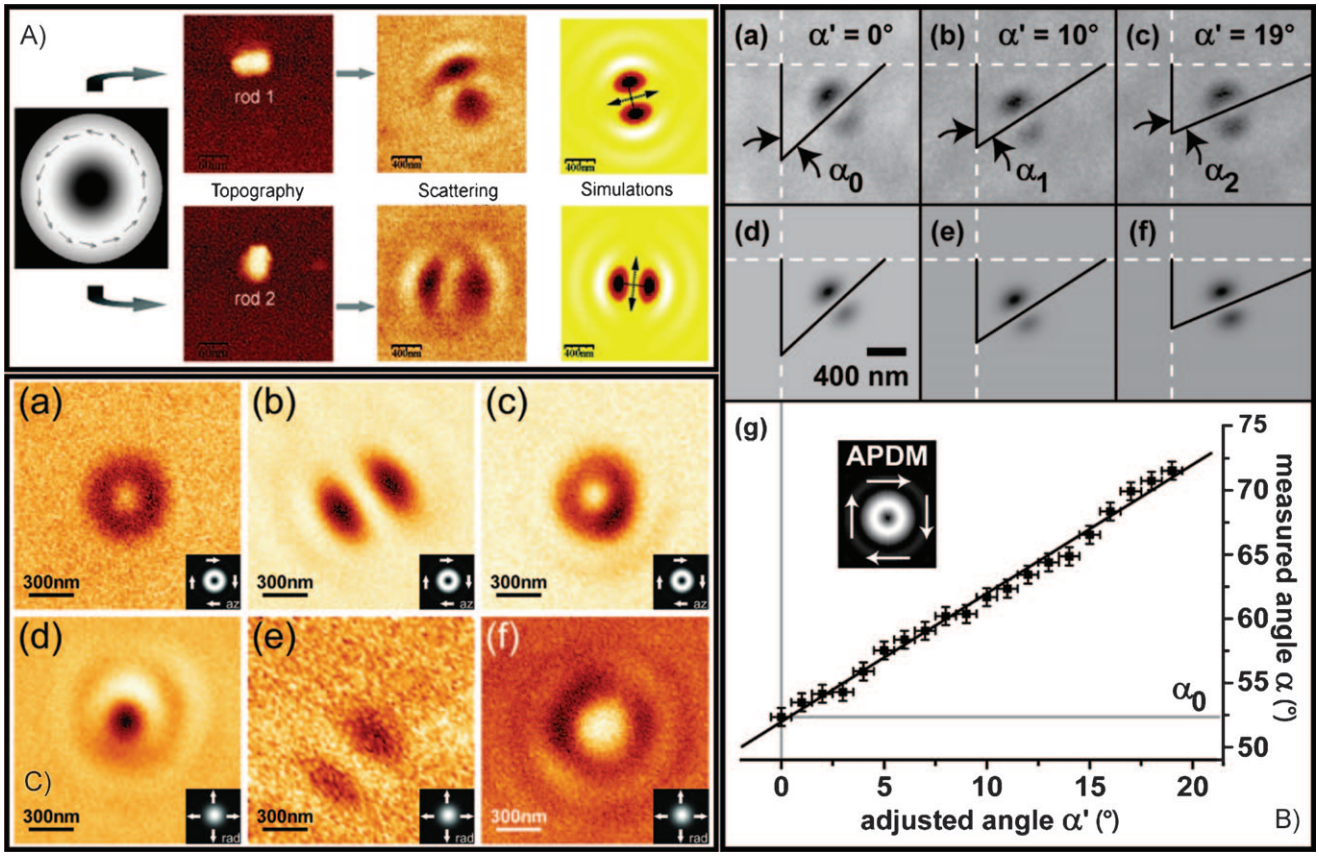

Figure 10. Scattering images of single metal nanoparticles illustrating the potential of confocal interference scattering microscopy with doughnut modes (CISM-DM). A) Topography (180×180 nm^2) and corresponding scattering images (2×2 μm^2) from two individual gold nanorods (APDM at 633 nm). Note that the experimental two-lobed patterns directly reveal the particle's orientation and nicely agree with the theoretical simulations. B) The orientation can be determined with a high accuracy of approximately 0.5°. Scattering images of the same silver nanorod, while the sample is rotated from picture to picture by around 10° [a)–c) experimental data, d)–f) fitted data, g) plot of the measured angle α versus the adjusted angle α']. C) Gold nanoparticles of different shapes can be distinguished by their scattering patterns a),d) sphere, b),e) rod, c),f) triangle.
A) Reprinted in part, with permission from Ref. [11a]. Copyright 2006 American Chemical Society. B) Reprinted with permission from Ref. [74].
C) Reprinted with permission from Ref. [43].

the sample interface is detected. The detected signal is caused by interference between the excitation light reflected at the sample interface and the one elastically scattered by the particle.[75]

The optical properties of noble-metal nanorods can be finely tuned by adjusting their size and hence they are extremely interesting for light-microscopy applications. The particles show a strong anisotropic polarizability, because the plasmon resonances for the two main axes differ. Usually, the resonance for the short axis is in the blue to green region while the one for the long axis is red shifted and varies with the aspect ratio (the ratio of the length over the width). It is situated further in the red the longer the particle is. Hence, brought into the focus of an APDM or RPDM at 633 nm, the particle plasmons of the long axis are mainly excited inducing a pronounced dipole moment mapping the particle's orientation. The images of particles laying flat on a glass surface are strongly reminiscent of those resulting from single molecules with a lateral dipolar orientation. Because of destructive interference, however, the image contrast might be reversed. Experimental results are shown in Figure 10A. The orientations of two individual gold nanorods are given by the in-situ topography data, in addition, the experimental confocal scattering images of the same particles upon excitation with an APDM are shown. Similar two-lobed patterns are acquired with a RPDM (Figure 10C, part d). The two-lobed patterns directly visualize the particles' orientations in a single confocal scan.[11a] Reproducing the experimental patterns with a 2D fit function to extract the orientation, an excellent precision well below 1° was found (Figure 10B).[74] For particles embedded in liquids, we could recently show that it is also possible to track rotations of nanorods, even without a translation of the particle.[21b] The observed spontaneous reorientation of a single gold nanorod in aqueous environment[21b] could not have been detected with standard light microscopy.

Particles of different shapes can be distinguished, as shown in Figure 10C. An isotropic scatterer, such as a gold nanosphere acting as a point-like probe maps the intensity distribution of the excitation beam. Hence, a sphere can be easily distinguished from a nanorod or a gold nanotriangle which gives distorted patterns compared to those of spheres.[11b]

Note that all this information from the nanoscale is accessible with a diffraction-limited and simple confocal imaging technique without any need for sophisticated data analysis. A remarkable benefit of the technique is its extraordinary precision in orientational determination for metal nanorods. Similar results are achievable for fluorescent molecules.

6. Doughnut Modes and Silica Nanoparticles

Single SiO_2 nanoparticles (NPs), for which the photoluminescence (PL) originates from defect states in the silica structure, have a stable linear transition dipole moment.[12] Therefore, they should give similar images to those of single molecules. Using both azimuthally and radially polarized light for excitation, the 3D orientation of the dipole moment has been imaged. Figure 11 shows a series of experimental two-lobed PL patterns from single NPs upon excitation with an APDM, recorded one after the other.[12] Rare dynamic effects, such as PL intermittency and flipping of the transition dipole moment, could be observed, although the NPs were fixed in a polymer matrix.

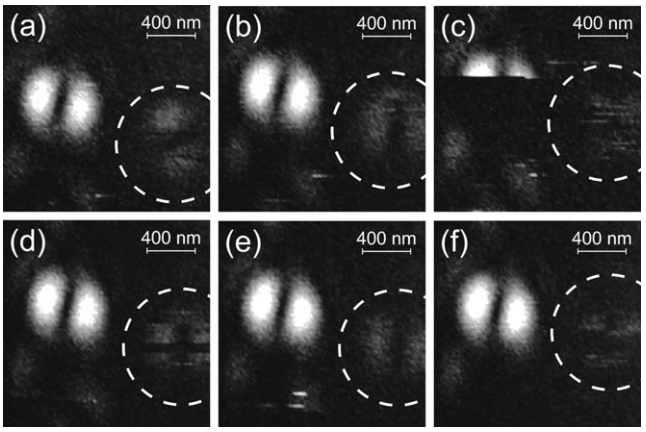

Figure 11. Images of SiO_2 nanoparticles (NPs) embedded in a polystyrene matrix and excited with an APDM ($\lambda = 488$ nm). The images a)–f) reveal the same image section of a series of pictures recorded one after the other every 100 s. Each image essentially shows two NPs, one appearing as a bright two-lobed pattern and a fainter one marked by the dashed circle. The following dynamical processes are observed: image (c) reveals photoluminescence (PL) intermittency of the brighter NP (also called blinking). Blinking is also observed for the fainter NP in image (d). In addition, we observe sudden flipping of the transition dipole moment of the fainter NP as can be seen by comparing images (a) and (b) as well as (e) and (f). Adapted with permission from Ref. [12]. Copyright 2009 American Chemical Society.

Different types of patterns, such as the ones in the case of single-molecule fluorescence,[6a] have been found using a RPDM for excitation,[12] allowing the 3D dipolar orientation to be determined. In addition, blinking of the brighter NP is observed in Figure 11c as well as for the fainter one (encircled) in Figure 11d. In addition, the fainter particle shows flipping of the transition dipole moment (Figure 11a,b).[12]

The orientation of the absorption and emission dipole could be shown to be parallel. This result leads to the important conclusion that the PL photon arises from the very defect that was excited.

7. Doughnut Modes in Microresonators

Metallic cavities, that is, microresonators, have been widely studied by the optics, laser physics, quantum optics, and physical chemistry communities.[76] Although a detailed overview about the impact of microresonators on scientific research is not the purpose of this Review, surely these systems have been and still are playing an important role in the investigation of the interaction between electromagnetic fields and matter, especially on the single-molecule level. In this wide frame, Steiner et al. have developed and charac-

terized a novel metallic microresonator device that allows the distance between the cavity silver mirrors to be tuned with nanometer precision.[13a] This unique and powerful device has been used to study and control the optical properties of nanoemitters, for example, to produce cavity-controlled spectra and decay curves of single molecules interacting at room temperature with the first longitudinal mode of a Fabri–Perot interferometer[13a] or to study quantitatively the effect of the microresonator-induced optical confinement on the optical properties of individual or an ensemble of nanoemitters.[77]

Exploiting the same system, Khoptyar et al. have studied the field distribution produced by a RPDM and an APDM in a microcavity by comparing the fluorescence patterns of point-like beads with theoretical calculations.[13b] Subsequently, Gutbrod et al. studied the field produced by a RPDM as a function of the cavity length. It was found that the special spatial field distribution of a RPDM in a cavity allows localizing a fluorescence emitter with subresolution precision ($\lambda/60$).[13c] Finally, Gutbrod et al. demonstrated that a RPDM can be successfully used to localize and to determine the orientation of individual molecules placed in a cavity.[78] Although the precision of this determination is not extremely high, RPDMs might be used to characterize and to optimize the interaction of FRET pairs.

8. Doughnut Modes for Trapping and Tweezing

Since optical trapping was first experimentally demonstrated by Ashkin in 1970,[79] it has found wide applications in physics, chemistry, and biology. Applications range from cooling and trapping of neutral atoms[80] to optical tweezing and manipulation of single molecules, nano- and microparticles[79,81] as well as biological objects (e.g. live bacteria and viruses,[82] cell compartments, or entire cells[83]).

In the following, the benefits resulting from the implementation of DMs in trapping applications are summarized. A short general discussion of the trapping principle is given since it is not always intuitively straightforward. The objects to be trapped normally have a higher refractive index than their surroundings. Thus, the particles are drawn into the focus of a laser beam, the so-called optical trap or tweezers. Typical particle sizes range from 200 to 500 nm, but also diameters of a few times λ or down to tens of nanometer are feasible.[84] As the laser beam and the sample are shifted relative to each other, the trapped object follows the focal spot and can be released from the trap at will.

The movement of the particle can be explained equally well either by the radiation pressure it experiences or by the momentum transfer from the incident photons knocking into it. The optical forces are small and balanced under normal conditions. Close to a tight laser focus, however, they can become directed and large enough to overwhelm Brownian motion and gravity, as well as the buoyancy force. Naturally, overpowering these forces is necessary to form a stable trap. For historic reasons, the force is normally decomposed into two components, the scattering force and the gradient force. The scattering force results from the fact that the object is hit by photons from one side only, therefore, the light pushes the particle in its direction of propagation and thus out of the focus. The gradient force is caused by the inhomogeneous electric field, achieved by tight focusing. The field fluctuations induce oscillating dipoles in the particles which in turn interact with the electric field and cause the gradient force. Therefore, the gradient force is a function of the polarizability of the particle and the optical intensity gradient and pulls the object into the trap. To increase the trapping efficiency, it is necessary to optimize the ratio of gradient over scattering force.

Only high angular components contribute to the electromagnetic field generated by focusing DMs with a high *NA* lens. DMs have been proposed for optical trapping[14f,22c,81a,85] because rays parallel to the axes contribute more to the scattering force whereas rays under higher angles mainly account for the gradient force. The scattering force being caused by reflection depends on the polarization of the incident light. Therefore, it can be minimized by p-polarization, such as that provided by a focused RPDM. Moreover, the longitudinal component of the beam is focused more strongly than a linearly polarized beam which should further increase the trapping efficiency. For these reasons, a RPDM promises to be close to the optimal beam for trapping applications. However, the resulting trapping efficiency predicted in theoretical publications is contradictory and remarkably different, depending on the applied computational theory. Stronger trapping forces on dielectric particles have been predicted[85a,b] and the improved efficiency should even allow for stable trapping of metallic Rayleigh particles.[85a] Both calculations in the ray optics regime and using rigorous electromagnetic theory suggested higher trapping efficiencies for a RPDM compared to a Gaussian beam.[85b,c] In contrast, for calculations incorporating plane waves, the trapping efficiency highly depends on the particle size.[86] Following these results, the RPDM should be only favorable for larger particles on the order of the wavelength to several micrometers.[86]

In general, trapping applications should benefit from the use of any doughnut shaped beam. In the longitudinal direction, 20% higher trapping forces have been reported compared to a linearly polarized Gaussian beam.[14a] However, lateral trapping is not improved with such DMs.[87] Nevertheless, many standard applications can profit from the application of DMs,[14b–f] but they are especially useful for the trapping of particles which are hard to trap with the standard technique. This includes the successful trapping of low refractive index, absorbing, and highly reflective particles.[14b–e,15a] Simultaneous trapping of high- and low-refractive index particles in the same DM has also been demonstrated.[15b]

To date, the experimental work in trapping applications with radially polarized light has just begun, however, calcite microparticles could be rotated using a RPDM.[14g] Although the light was not tightly focused, the presented data is promising for trapping applications. In contrast to an anisotropic particle spinning around an axis independent of the laser beam in the focus of circularly or elliptically polarized light,[88] the particles spun around the beam's axis, that is, the

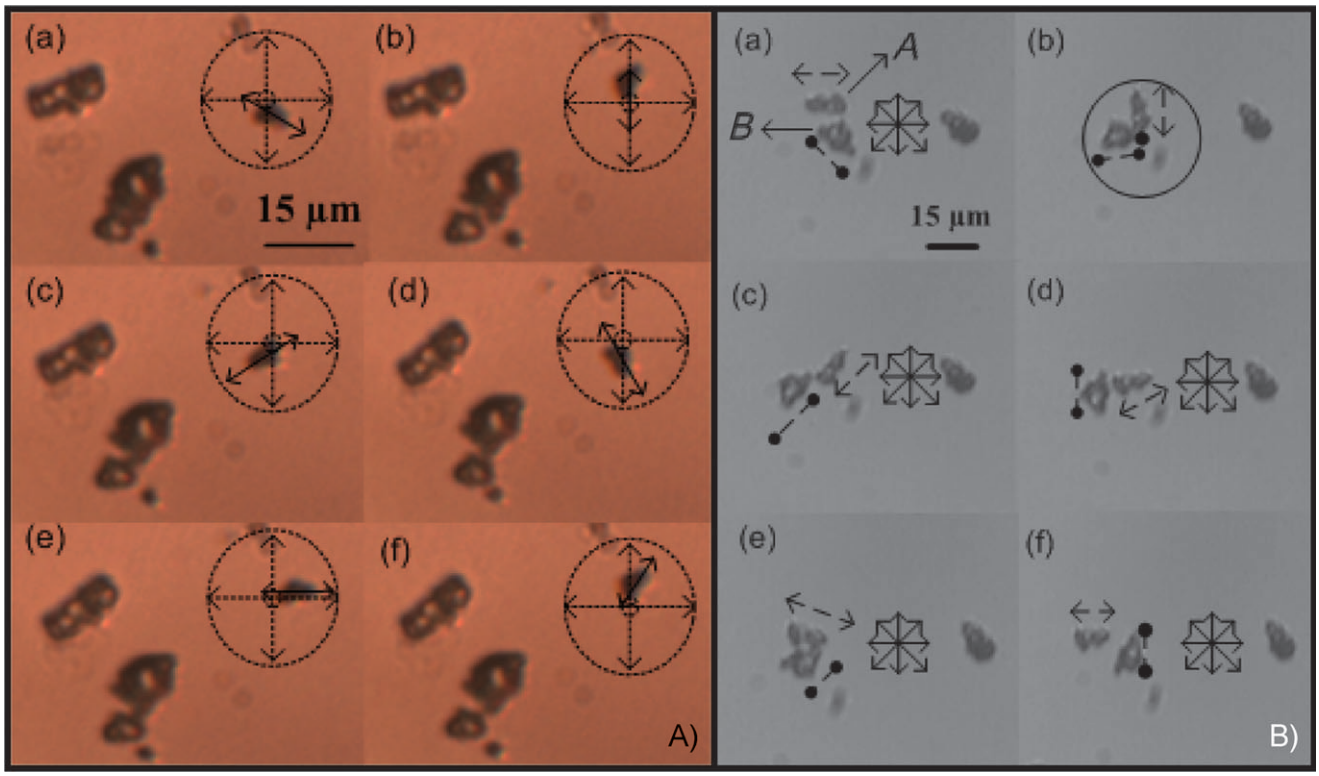

Figure 12. A) Polarization-induced torque on anisotropic particles by a RPDM setting it to rotate (in an anticlockwise direction) around the beam. B) A system of two anisotropic microparticles in a RPDM. Particle *A* rotates in a clockwise direction and particle *B* in an anticlockwise direction. Reprinted with permission from Ref. [14g]. Copyright 2007, American Institute of Physics.

optical axis (see Figure 12).[14g] The spinning direction was observed not to be predictable which was ascribed to the particle shape, size, and dimension.[14g]

It should be mentioned that an APDM can also be suitable for trapping applications since stable trapping of tungsten particles has been shown.[20b]

9. Doughnut Modes in Near-Field Microscopy

After the development of near-field microscopy in the early 1980s,[3] the field has undergone great development and it has been demonstrated that optical microscopy can reach far beyond the diffraction limit. The highest resolutions are achieved with tip-enhanced near-field optical microscopy (TENOM) which utilizes—in contrast to aperture scanning near-field microscopy—extremely sharp metal tips (usually made of gold or silver). These tips are brought into the focus of a RPDM where the longitudinal field excites the electrons in the tip to oscillate along the optical axis. At the plasmon resonance (or close to it), the electrons are efficiently pumped into the tip apex. High field enhancements are achieved at the end of the tip and the tip itself acts as an antenna. Close to an interface, tip-enhanced fluorescence (TEF) or tip-enhanced Raman scattering (TERS) can be observed. These enhancement effects promise to further increase the sensitivity in optical microscopy and spectroscopy. The actual realization of the microscope setup varies, depending on the specific experimental demands. Most near-field setups are in principle based on the confocal microscope and therefore feature objectives as focusing and collecting element. As a consequence, the characterization of opaque samples is limited. However, replacing the objective with a parabolic mirror allows these limitations to be overcome. Another benefit of such a setup is that the longitudinally polarized field in focus, which excites the electron oscillation in the sharp metal tip, is much stronger for a parabolic mirror than a microscope objective of comparable *NA*.[6b] Using such a setup, extraordinarily high field enhancements have been achieved in the tunable gap of a 3D bowtie antenna system formed by a sharp metal probe and a gold nanocone.[89] However, note that the technique is limited to the study of surfaces. To treat near-field optics in more detail is beyond the scope of this Review. It has been the topic of numerous Reviews and books.[21a,90] Novel developments in TENOM have been reviewed in a recent article by Hartschuh.[4]

10. Doughnut Modes for Surface Plasmon Resonance Imaging

The phenomenon of surface plasmon resonance (SPR) excitation in thin metal films (typically 50 nm Ag) has found wide applications in optical sensing.[91] Rothenhäusler et al. exploited this effect for surface plasmon microscopy (SPM).[92] Contrary to standard microscopy techniques with light sources such as lamps and lasers, surface plasmon polaritons (SPPs) are used for excitation. These non-radiative

electromagnetic modes travel along an interface (metal-dielectric) as surface bound waves. Since the intensity perpendicular to the interface decays exponentially, the technique is sensitive to the direct environment of the metal film. The propagation length of the SPP, however, basically limits the lateral resolution to a few (tens of) micrometers.[93] To improve the resolution, tightly focused laser beams have been used to locally excite SPPs in an area close to the spot size of the focused beam. Kano et al. carried out numerical simulations and experiments to investigate the influence of polarization on the electric field distribution.[16g,94] These results were experimentally demonstrated for linearly polarized light showing local excitation in an area of only $0.5 \times 0.5\ \mu m^2$.[16g]

Since the SPPs are excited by the longitudinal component, a RPDM should perform better both in terms of localization and of intensity as has been shown theoretically and experimentally.[16a,g] Although perfect agreement of theory and experiment could not yet be achieved, evanescent non-diffracting Bessel beams were generated by SPR excitation with a RPDM.[16b–e] Such beams could serve as virtual probes for SPR imaging as shown in an experimental proof-of-concept.[16f] Cells and their substrate contacts were successfully imaged providing a map of refractive indices (see Figure 13).[16f]

Recently, also first experimental results on two-photon luminescence induced by such a virtual probe have been published.[95] These results are promising regarding scanning-probe techniques without the need of a material probe to penetrate the enclosed environment. However, note that the technique is limited to the study of a region close to the metallic film. In conclusion, a RPDM can be used to increase the lateral resolution for SPR imaging and refractive-index sensing and thus provide extra information supporting other light-microscopy techniques.

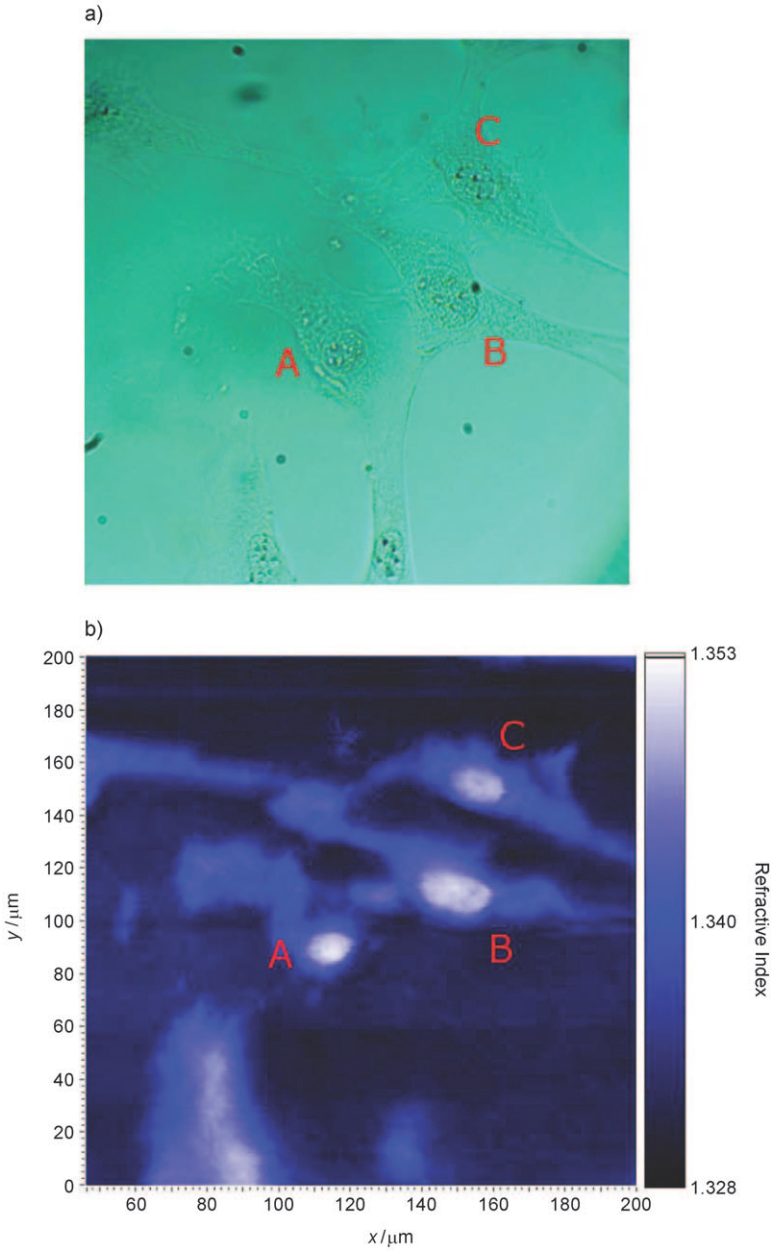

Figure 13. a) Light microscopy image of human 3T3 fibroblast cells, b) obtained refractive index map of the same group of cells scanned by a virtual SPR probe. The same sample area can be easily recognized underscoring the potential of the technique to provide extra information supporting other light-microscopy methods. Reprinted with permission from Ref. [16f].

11. Doughnut Modes for Nonlinear-Optics Microscopy

When a pulsed laser of high intensity and long wavelength is tightly focused on a non-amorphous medium, second harmonic generation (SHG) may occur. In this process, two photons have to simultaneously interact with a molecule which has a symmetry that should not be centrosymmetric. The photons are purely elastically scattered and light of half the wavelength is emitted (the energy is conserved). Hence, changing the excitation wavelength also alters the emitted color. In addition, the momentum is conserved, that is, the vectoral sum of the polarization directions has to match the dipole moment orientation. Since radially and azimuthally polarized light offer different orientations, they are good candidates for applications in SHG.

Biss and Brown showed that SHG at smooth metal and semiconductor surfaces as well as thin films is strongest for a RPDM compared to linearly, circularly, and azimuthally polarized light.[96] They explained this phenomenon with the strength of the longitudinal field component in focus decreasing in the order given above.[96] Moreover, the RPDM offers higher spatial resolution than the other beams studied.[96]

The use of a RPDM in SHG microscopy has been suggested to detect the 3D molecular orientation.[17a,b] A technical benefit of the suggested setup for mode conversion in Ref. [17b] is that it allows for fast mode switching which appears to be promising especially for commercial setups.

Biological tissue rich in collagen with a preferred molecular orientation along the optical axis showed a higher SHG contrast upon excitation with radially polarized light than

with light polarized in the sample plane.[17a,c] Recently, it was shown that this also holds true for a self-assembled monolayer (SAM) on a gold surface, where the molecular dipoles show a preferentially longitudinal orientation.[97] Yew and Sheppard revealed that both the longitudinal and transverse components of the electric field in focus have to be taken into account to explain their experimental SHG data.[98] Although to date, to our knowledge, only ensemble measurements were realized, the technique generally promises to allow for single-molecule sensitivity. Furthermore, the SHG signal produced by a self-assembled monolayer on gold is enhanced using a RPDM.[97] On the other hand, SHG from a crystal can also be used to produce radially polarized light.[37c] Additionally, theoretic simulations suggest that even third harmonic generation (THG) from a bulk sample under defined conditions should be detectable.[99] Moreover, RPDMs are important to improve the resolution in two-photon microscopy.[100] Accordingly, also in THG microscopy, a better spatial resolution is expected.[99]

Finally, RPDMs influence another nonlinear optical technique: two-photon fluorescence correlation spectroscopy (2p-FCS). They allow for single-molecule studies with higher sample concentrations since the intensity threshold for two-photon excitation reduces the effective focal volume. As a consequence, the side-lobes of the electric field distribution no longer contribute to the sample excitation and the effective focal volume is smaller than for the standard, one-photon excitation.[101]

12. Doughnut Modes for Micromechanics Applications

High-power lasers play an important role in the industrial cutting and drilling of metals. Thus, there is substantial interest in further development of the laser sources and beams. Regarding micromechanics applications, theoretical simulations suggested that a RPDM should be up to two times more efficient than a plane p-polarized beam or a circularly polarized one, both of which are used in standard laser drilling and cutting techniques.[18a,102] Experimental results on thin metal sheets indeed showed an increased efficiency for a RPDM. However, further experiments showed that increasing the efficiency with DMs is a problem involving a much more complex dependency. It could be shown that both an APDM and a RPDM are more efficient than linearly and circularly polarized beams. Depending on the metals' optical properties and the metal thickness, the APDM can be up to four-times more efficient in mild steel overwhelming even the RPDM in efficiency.[18b] Surprisingly, Meier et al. also showed that the holes drilled with an APDM can be much smaller than those of a RPDM of the same focus size under special conditions.[18b]

To drill interconnected microholes (microvias) in silicon, a significantly better performance of a RPDM compared to circularly polarized light has been reported.[103] The improved ablation rate of up to two[103] exactly confirmed the value predicted in Ref. [18a]. The diameter of the drilled holes was reduced by 30% whereas the higher efficiency of the RPDM depended on the repetition rate and thus the energy of the applied pulses. The microvia diameter was found to decrease with the pulse energy (increasing repetition rate). The energy dependence of the ablation rate was found to be stronger for a RPDM than for other p-polarized beams. The depth-profile also depended strongly on the pulse energy where the taper angle reduced decreasing this measure. Straight sidewalls were achieved with an accompanying cleaner surface with less debris to be found, aiding the cleaning procedure after the cutting procedure.[103]

13. Summary and Outlook

In the last few years, doughnut modes (DMs) have become a focus of interest in different fields of science. Numerous techniques have been developed to produce ring-shaped beams of which only a few could be covered herein. Their physical properties have been widely studied, with special emphasis on their behavior upon tight focusing. These fundamental studies revealed extraordinary properties of DMs which can be exploited in various ways. As an example, the implementation of DMs in light microscopy allowed Abbe's famous diffraction limit to be circumvented with STED microscopy. In tip-enhanced near-field optical microscopy (TENOM), sharp metal tips are illuminated with DMs of special polarization, so-called radially polarized DMs (RPDMs). Plasmon resonances can be excited in the metal tips with the strong longitudinally polarized fields these modes produce upon tight focusing.

In the shadow of such well known applications, a number of new applications have evolved which mainly use radially and azimuthally polarized light. Such applications have been summarized herein ranging from the implementation in different light-microscopy methods and related techniques, such as trapping and tweezing to micromechanics applications.

In standard light microscopy, radially polarized light can be used to increase the lateral resolution because of the special properties upon focusing. However, this is only one aspect. These modes have also drawn the attention of researchers who are active in the field of single-molecule microscopy and spectroscopy. From a fundamental point of view, single molecules can be utilized to probe the special field distribution these modes provide in focus. On the other hand, knowing the field distribution reveals additional information about single molecules, such as their orientation. In special cases, chemical reactions can even be watched on the single-molecular level. Both with an APDM and a RPDM, orientational information of single molecules or more generally speaking single nanoobjects, for example, noble-metal or silica nanoparticles, can be achieved. Naturally, this is not the only technique to extract orientational information. To clarify the power of DMs in light microscopy and to underline the advantages which can be drawn from their implementation, other well established techniques to determine the orientation of single molecules, such as defocused imaging and polarization sensitive methods were summarized.

However, starting from single molecules, single nanoobjects might be of wider interest. Again, azimuthally and radially polarized light provide access to additional information not directly accessible with standard light microscopy. As an example, metal nanoparticles of different shapes can be distinguished using DMs. The only modification necessary compared to standard confocal microscopy is the mode conversion (MC) for which a variety of suitable techniques is already available as partly summarized herein. Therefore, the additional technical effort is negligible. Recently, a laser scanning microscope with variable laser polarizations was reported[104] which could certainly also be used for similar experiments especially if applied to biological specimens. Such a system can be considered as a prototype of a commercially available setup.

Also further advanced microscopy techniques, such as surface plasmon resonance (SPR) imaging or second harmonic generation (SHG) microscopy, profited from the implementation of DMs as explained in this Review. In addition, techniques closely related to microscopy have also benefited, such as trapping and tweezing or micromechanics applications for industrial drilling and cutting of metals.

We have also to consider that this Review was dedicated mainly to first-order RPDMs or APDMs. Nowadays, second- and third -order DMs are beginning to be discovered[39a,b] which might push the optical resolution limit even further and provide versatile tools for nanotechnology. As an example, by tuning the focusing properties of second-order RPDMs, it might be possible to build up an optical cage (a dark central zone in the focus surrounded by a strong electric field gradient).[39a,40a]

We believe that these applications are just the beginning of a long row of future techniques exploiting the favorable properties of DMs as the scientific community becomes more and more aware of these beams. Although most of the applications shown herein are related to microscopy, the results already achieved show pathways in many directions and are extremely promising for the next years. DMs provide a link between different fields of science which are generally considered to be far away from each other. This link reaches from pure optics and light microscopy through the broad field of nanotechnology to industrial applications of cutting metals.

As has been shown in this Review, the ice has been broken and we are now experiencing the beginning of a process which might result in a true avalanche of applications and knowledge.

Supportive experimental as well as stimulating discussions with Frank Wackenhut is highly appreciated. Financial support by the Deutsche Forschungsgemeinschaft DFG and the Landesstiftung Baden-Württemberg is gratefully acknowledged.

Received: September 17, 2010
Revised: December 15, 2010
Published online: May 17, 2011

[1] S. W. Hell, J. Wichmann, *Opt. Lett.* **1994**, *19*, 780 – 782.
[2] S. W. Hell, *Science* **2007**, *316*, 1153 – 1158.
[3] a) D. W. Pohl, W. Denk, M. Lanz, *Appl. Phys. Lett.* **1984**, *44*, 651 – 653; b) A. Lewis, M. Isaacson, A. Harootunian, A. Muray, *Ultramicroscopy* **1984**, *13*, 227 – 231.
[4] a) A. Hartschuh, *Angew. Chem.* **2008**, *120*, 8298 – 8312; *Angew. Chem. Int. Ed.* **2008**, *47*, 8178 – 8191.
[5] a) S. Quabis, R. Dorn, M. Eberler, O. Glöckl, G. Leuchs, *Opt. Commun.* **2000**, *179*, 1 – 7; b) R. Dorn, S. Quabis, G. Leuchs, *Phys. Rev. Lett.* **2003**, *91*, 233901; c) J. Stadler, C. Stanciu, C. Stupperich, A. J. Meixner, *Opt. Lett.* **2008**, *33*, 681 – 683; d) A. Yanai, U. Levy, *Opt. Express* **2009**, *17*, 924 – 932; e) G. M. Lerman, A. Yanai, U. Levy, *Nano Lett.* **2009**, *9*, 2139 – 2143.
[6] a) L. Novotny, M. R. Beversluis, K. S. Youngworth, T. G. Brown, *Phys. Rev. Lett.* **2001**, *86*, 5251 – 5254; b) M. A. Lieb, A. J. Meixner, *Opt. Express* **2001**, *8*, 458 – 474.
[7] a) J. Waluk, *Acc. Chem. Res.* **2006**, *39*, 945 – 952; b) H. Piwoński, C. Stupperich, A. Hartschuh, J. Sepioł, A. Meixner, J. Waluk, *J. Am. Chem. Soc.* **2005**, *127*, 5302 – 5303; c) H. Piwoński, A. Hartschuh, N. Urbańska, M. Pietraszkiewicz, J. Sepioł, A. J. Meixner, J. Waluk, *J. Phys. Chem. C* **2009**, *113*, 11514 – 11519.
[8] a) J. Jasny, J. Sepioł, *Chem. Phys. Lett.* **1997**, *273*, 439 – 443; b) J. Sepioł, J. Jasny, J. Keller, U. P. Wild, *Chem. Phys. Lett.* **1997**, *273*, 444 – 448; c) R. M. Dickson, D. J. Norris, W. E. Moerner, *Phys. Rev. Lett.* **1998**, *81*, 5322 – 5325; d) A. P. Bartko, R. M. Dickson, *J. Phys. Chem. B* **1999**, *103*, 3053 – 3056; e) A. P. Bartko, R. M. Dickson, *J. Phys. Chem. B* **1999**, *103*, 11237 – 11241; f) M. Böhmer, J. Enderlein, *J. Opt. Soc. Am. B* **2003**, *20*, 554 – 559; g) D. Patra, I. Gregor, J. Enderlein, *J. Phys. Chem. A* **2004**, *108*, 6836 – 6841.
[9] a) E. Betzig, R. J. Chichester, *Science* **1993**, *262*, 1422 – 1425; b) A. G. T. Ruiter, J. A. Veerman, M. F. Garcia-Parajo, N. F. van Hulst, *J. Phys. Chem. A* **1997**, *101*, 7318 – 7323; c) F. Güttler, J. Sepiol, T. Plakhotnik, A. Mitterdorfer, A. Renn, U. P. Wild, *J. Lumin.* **1993**, *56*, 29 – 38; d) T. Ha, T. Enderle, D. S. Chemla, P. R. Selvin, S. Weiss, *Phys. Rev. Lett.* **1996**, *77*, 3979 – 3982; e) K. D. Weston, L. S. Goldner, *J. Phys. Chem. B* **2001**, *105*, 3453 – 3462; f) M. Vacha, M. Kotani, *J. Chem. Phys.* **2003**, *118*, 5279 – 5282; g) G. S. Harms, M. Sonnleitner, G. J. Schütz, H. J. Gruber, T. Schmidt, *Biophys. J.* **1999**, *77*, 2864 – 2870.
[10] a) B. Sick, B. Hecht, L. Novotny, *Phys. Rev. Lett.* **2000**, *85*, 4482 – 4485; b) M. A. Lieb, J. M. Zavislan, L. Novotny, *J. Opt. Soc. Am. B* **2004**, *21*, 1210 – 1215.
[11] a) A. V. Failla, H. Qian, H. Qian, A. Hartschuh, A. J. Meixner, *Nano Lett.* **2006**, *6*, 1374 – 1378; b) T. Züchner, A. V. Failla, A. Hartschuh, A. J. Meixner, *J. Microsc.* **2008**, *229*, 337 – 343.
[12] A. M. Chizhik, A. I. Chizhik, R. Gutbrod, A. J. Meixner, T. Schmidt, J. Sommerfeld, F. Huisken, *Nano Lett.* **2009**, *9*, 3239 – 3244.
[13] a) M. Steiner, F. Schleifenbaum, C. Stupperich, A. V. Failla, A. Hartschuh, A. J. Meixner, *ChemPhysChem* **2005**, *6*, 2190 – 2196; b) D. Khoptyar, R. Gutbrod, A. Chizhik, J. Enderlein, F. Schleifenbaum, M. Steiner, A. J. Meixner, *Opt. Express* **2008**, *16*, 9907 – 9917; c) R. Gutbrod, A. Chizhik, A. Chizhik, D. Khoptyar, A. J. Meixner, *Opt. Lett.* **2009**, *34*, 629 – 631.
[14] a) S. Sato, M. Ishigure, H. Inaba, *IET Electron. Lett.* **1991**, *27*, 1831 – 1832; b) A. Ashkin, J. M. Dziedzic, *Appl. Phys. Lett.* **1974**, *24*, 586 – 588; c) H. He, N. R. Heckenberg, H. Rubinsztein-Dunlop, *J. Mod. Opt.* **1995**, *42*, 217 – 223; d) H. He, M. E. J. Friese, N. R. Heckenberg, H. Rubinsztein-Dunlop, *Phys. Rev. Lett.* **1995**, *75*, 826 – 829; e) K. T. Gahagan, G. A. Swartzlander, Jr., *Opt. Lett.* **1996**, *21*, 827 – 829; f) M. E. J. Friese, H. Rubinsztein-Dunlop, N. R. Heckenberg, E. W. Dearden, *Appl. Opt.* **1996**, *35*, 7112 – 7116; g) B. P. S. Ahluwalia, X.-C. Yuan, K. J. Moh, J. Bu, *Appl. Phys. Lett.* **2007**, *91*, 171102.
[15] a) V. G. Shvedov, A. S. Desyatnikov, A. V. Rode, W. Krolikowski, Y. S. Kivshar, *Opt. Express* **2009**, *17*, 5743 – 5757; b) K. T.

Gahagan, G. A. Swartzlander, Jr., *J. Opt. Soc. Am. B* **1999**, *16*, 533 – 537.
[16] a) K. Watanabe, N. Horiguchi, H. Kano, *Appl. Opt.* **2007**, *46*, 4985 – 4990; b) T. Grosjean, D. Courjon, *J. Microsc.* **2001**, *202*, 273 – 278; c) Q. Zhan, *Opt. Lett.* **2006**, *31*, 1726 – 1728; d) T. Grosjean, D. Courjon, D. van Labeke, *J. Microsc.* **2003**, *210*, 319 – 323; e) W. Chen, Q. Zhan, *Opt. Lett.* **2009**, *34*, 722 – 724; f) K. J. Moh, X.-C. Yuan, J. Bu, S. W. Zhu, B. Z. Gao, *Opt. Express* **2008**, *16*, 20734 – 20741; g) H. Kano, S. Mizuguchi, S. Kawata, *J. Opt. Soc. Am. B* **1998**, *15*, 1381 – 1386.
[17] a) K. Yoshiki, M. Hashimoto, T. Araki, *Jpn. J. Appl. Phys.* **2005**, *44*, L1066 – L1068; b) M. Hashimoto, K. Yamada, T. Araki, *Opt. Rev.* **2005**, *12*, 37 – 41; c) K. Yoshiki, K. Ryosuke, M. Hashimoto, N. Hashimoto, T. Araki, *Opt. Lett.* **2007**, *32*, 1680 – 1682.
[18] a) V. G. Niziev, A. V. Nesterov, *J. Phys. D* **1999**, *32*, 1455 – 1461; b) M. Meier, V. Romano, T. Feurer, *Appl. Catal. A* **2007**, *86*, 329 – 334.
[19] a) L. Novotny, B. Hecht, *Principles of Nano-Optics*, University Press, Cambridge, **2006**; b) S. Quabis, R. Dorn, G. Leuchs, *Appl. Catal. B* **2005**, *81*, 597 – 600; c) S. Quabis, R. Dorn, M. Eberler, O. Glöckl, G. Leuchs, *Appl. Catal. B* **2001**, *72*, 109 – 113.
[20] a) N. Davidson, N. Bokor, *Opt. Lett.* **2004**, *29*, 1318 – 1320; b) K. Sakai, S. Noda, *IET Electron. Lett.* **2007**, *43*, 107 – 108.
[21] a) Ref. [19a]; b) T. Züchner, F. Wackenhut, A. V. Failla, A. J. Meixner, *Appl. Surf. Sci.* **2009**, *255*, 5391 – 5395.
[22] a) K. S. Youngworth, T. G. Brown, *Opt. Express* **2000**, *7*, 77 – 87; b) N. K. Viswanathan, V. V. G. Inavalli, *Opt. Lett.* **2009**, *34*, 1189 – 1191; c) Q. Zhan, *J. Opt. A* **2003**, *5*, 229 – 232; d) G. M. Lerman, Y. Lilach, U. Levy, *Opt. Lett.* **2009**, *34*, 1669 – 1671.
[23] a) G. C. Dente, *Appl. Opt.* **1979**, *18*, 2911 – 2912; b) R. A. Chodzko, S. B. Mason, E. B. Turner, W. W. Plummer, Jr., *Appl. Opt.* **1980**, *19*, 778 – 789; c) H. Kogelnik, T. Li, *Appl. Opt.* **1966**, *5*, 1550 – 1567; d) G. Machavariani, Y. Lumer, I. Moshe, A. Meir, S. Jackel, N. Davidson, *Appl. Opt.* **2007**, *46*, 3304 – 3310.
[24] a) D. Pohl, *Appl. Phys. Lett.* **1972**, *20*, 266 – 267; b) Y. Mushiake, K. Matsumura, N. Nakajima, *Proc. IEEE* **1972**, *60*, 1107 – 1109; c) M. A. Ahmed, J. Schulz, A. Voss, O. Parriaux, J.-C. Pommier, T. Graf, *Opt. Lett.* **2007**, *32*, 1824 – 1826; d) R. Oron, S. Blit, N. Davidson, A. A. Friesem, Z. Bomzon, E. Hasman, *Appl. Phys. Lett.* **2000**, *77*, 3322 – 3324; e) Y. Kozawa, S. Sato, *Opt. Lett.* **2005**, *30*, 3063 – 3065; f) T. Hirayama, Y. Kozawa, T. Nakamura, S. Sato, *Opt. Express* **2006**, *14*, 12839 – 12845; g) A. Ito, Y. Kozawa, S. Sato, *J. Opt. Soc. Am. B* **2009**, *26*, 708 – 712; h) F. Enderli, T. Feurer, *Opt. Lett.* **2009**, *34*, 2030 – 2032.
[25] T. A. Klar, S. Jakobs, M. Dyba, A. Egner, S. W. Hell, *Proc. Natl. Acad. Sci. USA* **2000**, *97*, 8206 – 8210.
[26] S. C. Tidwell, D. H. Ford, W. D. Kimura, *Appl. Opt.* **1990**, *29*, 2234 – 2239.
[27] a) S. C. Tidwell, G. H. Kim, W. D. Kimura, *Appl. Opt.* **1993**, *32*, 5222 – 5229; b) D. P. Biss, K. S. Youngworth, T. G. Brown, *Appl. Opt.* **2006**, *45*, 470 – 479.
[28] T. A. Klar, E. Engel, S. W. Hell, *Phys. Rev. E* **2001**, *64*, 066613.
[29] P. B. Phua, W. J. Lai, Y. L. Lim, B. S. Tan, R. F. Wu, K. S. Lai, H. W. Tan, *physics.optics* **2007**, *arXiv:0710.4979v1*.
[30] G. Machavariani, Y. Lumer, I. Moshe, A. Meir, S. Jackel, *Opt. Lett.* **2007**, *32*, 1468 – 1470.
[31] G. M. Lerman, U. Levy, *Opt. Lett.* **2008**, *33*, 2782 – 2784.
[32] M. Stalder, M. Schadt, *Opt. Lett.* **1996**, *21*, 1948 – 1950.
[33] M. Schadt, W. Helfrich, *Appl. Phys. Lett.* **1971**, *18*, 127 – 128.
[34] M. A. A. Neil, F. Massoumian, R. Juškaitis, T. Wilson, *Opt. Lett.* **2002**, *27*, 1929 – 1931.
[35] E. G. Churin, J. Hoßfeld, T. Tschudi, *Opt. Commun.* **1993**, *99*, 13 – 17.
[36] a) T. Grosjean, D. Courjon, M. Spajer, *Opt. Commun.* **2002**, *203*, 1 – 5; b) T. Grosjean, A. Sabac, D. Courjon, *Opt. Commun.* **2005**, *252*, 12 – 21; c) T. Grosjean, M. Suarez, A. Sabac, *Appl. Phys. Lett.* **2008**, *93*, 231106.
[37] a) Z. Bomzon, G. Biener, V. Kleiner, E. Hasman, *Opt. Lett.* **2002**, *27*, 285 – 287; b) J.-i. Hotta, H. Uji-i, J. Hofkens, *Opt. Express* **2006**, *14*, 6273 – 6278; c) S. Sato, Y. Kozawa, *Opt. Lett.* **2009**, *34*, 3166 – 3168.
[38] a) T. Grosjean, D. Courjon, *Phys. Rev. E* **2003**, *67*, 046611; b) R. K. Singh, P. Senthilkumaran, K. Singh, *J. Opt. Soc. Am. A* **2009**, *26*, 576 – 588; c) C. J. R. Sheppard, A. Choudhury, *Appl. Opt.* **2004**, *43*, 4322 – 4327; d) I. J. Cooper, C. J. R. Sheppard, M. Sharma, *Optik* **2002**, *113*, 293 – 298; e) D. G. Hall, *Opt. Lett.* **1996**, *21*, 9 – 11; f) R. H. Jordan, D. G. Hall, *Opt. Lett.* **1994**, *19*, 427 – 429.
[39] a) Y. Kozawa, S. Sato, *Opt. Lett.* **2006**, *31*, 820 – 822; b) Y. Kozawa, S. Sato, *J. Opt. Soc. Am. A* **2007**, *24*, 1793 – 1798; c) Q. Zhan, J. R. Leger, *Opt. Express* **2002**, *10*, 324 – 331; d) I. J. Cooper, M. Roy, C. J. R. Sheppard, *Opt. Express* **2005**, *13*, 1066 – 1071; e) Y. Lumer, I. Moshe, *Opt. Lett.* **2009**, *34*, 265 – 267; f) D. P. Brown, A. K. Spilman, T. G. Brown, R. Borghi, S. N. Volkov, E. Wolf, *Opt. Commun.* **2008**, *281*, 5287 – 5290; g) Y. Luo, B. Lü, *J. Opt. A* **2009**, *11*, 015707; h) R. Martínez-Herrero, P. M. Mejías, G. Piquero, V. Ramírez-Sánchez, *Opt. Commun.* **2008**, *281*, 1976 – 1980; i) S. Sato, Y. Kozawa, *J. Opt. Soc. Am. A* **2009**, *26*, 142 – 146; j) R. Borghi, M. Santarsiero, M. A. Alonso, *J. Opt. Soc. Am. A* **2005**, *22*, 1420 – 1431.
[40] a) G. Zhou, *J. Opt. Soc. Am. A* **2009**, *26*, 1654 – 1660; b) Y. Lumer, I. Moshe, A. Meir, Y. Paiken, G. Machavariani, S. Jackel, *J. Opt. Soc. Am. B* **2007**, *24*, 2279 – 2286.
[41] B. Richards, E. Wolf, *Proc. R. Soc. London Ser. A* **1959**, *253*, 358 – 379.
[42] E. Wolf, *Proc. R. Soc. London Ser. A* **1959**, *253*, 349 – 357.
[43] T. Züchner, A. V. Failla, M. Steiner, A. J. Meixner, *Opt. Express* **2008**, *16*, 14635 – 14644.
[44] C. Eggeling, C. Ringemann, R. Medda, G. Schwarzmann, K. Sandhoff, S. Polyakova, V. N. Belov, B. Hein, C. von Middendorff, A. Schonle, S. W. Hell, *Nature* **2009**, *457*, 1159 – 1162.
[45] J. Keller, A. Schönle, S. W. Hell, *Opt. Express* **2007**, *15*, 3361 – 3371.
[46] a) K. I. Willig, S. O. Rizzoli, V. Westphal, R. Jahn, S. W. Hell, *Nature* **2006**, *440*, 935 – 939; b) E. Engel, N. Huse, T. A. Klar, S. W. Hell, *Appl. Phys. B* **2003**, *77*, 11 – 17.
[47] M. Dyba, S. W. Hell, *Phys. Rev. Lett.* **2002**, *88*, 163901.
[48] M. C. Lang, T. Staudt, J. Engelhardt, S. W. Hell, *New J. Phys.* **2008**, *10*, 043041.
[49] N. Bokor, N. Davidson, *Opt. Commun.* **2008**, *281*, 5499 – 5503.
[50] M. Hofmann, C. Eggeling, S. Jakobs, S. W. Hell, *Proc. Natl. Acad. Sci. USA* **2005**, *102*, 17565 – 17569.
[51] G. Terakado, K. Watanabe, H. Kano, *Appl. Opt.* **2009**, *48*, 1114 – 1118.
[52] F. Lu, W. Zheng, Z. Huang, *Opt. Lett.* **2009**, *34*, 1870 – 1872.
[53] W. T. Tang, E. Y. S. Yew, C. J. R. Sheppard, *Opt. Lett.* **2009**, *34*, 2147 – 2149.
[54] M. Kreiter, M. Prummer, B. Hecht, U. P. Wild, *J. Chem. Phys.* **2002**, *117*, 9430 – 9433.
[55] J. Enderlein, E. Toprak, P. R. Selvin, *Opt. Express* **2006**, *14*, 8111 – 8120.
[56] M. A. Osborne, *J. Phys. Chem. B* **2005**, *109*, 18153 – 18161.
[57] A. P. Bartko, L. A. Peyser, R. M. Dickson, A. Mehta, T. Thundat, R. Bhargava, M. D. Barnes, *Chem. Phys. Lett.* **2002**, *358*, 459 – 465.
[58] W. Schroeyers, R. Vallée, D. Patra, J. Hofkens, S. Habuchi, T. Vosch, M. Cotlet, K. Müllen, J. Enderlein, F. C. De Schryver, *J. Am. Chem. Soc.* **2004**, *126*, 14310 – 14311.
[59] a) E. Toprak, J. Enderlein, S. Syed, S. A. McKinney, R. G. Petschek, T. Ha, Y. E. Goldman, P. R. Selvin, *Proc. Natl. Acad. Sci. USA* **2006**, *103*, 6495 – 6499; b) H. Uji-i, S. M. Melnikov, A.

Deres, G. Bergamini, F. De Schryver, A. Herrmann, K. Müllen, J. Enderlein, J. Hofkens, *Polymer* **2006**, *47*, 2511 – 2518.
[60] a) H. Sosa, E. J. G. Peterman, W. E. Moerner, L. S. B. Goldstein, *Nat. Struct. Biol.* **2001**, *8*, 540 – 544; b) E. J. G. Peterman, H. Sosa, L. S. B. Goldstein, W. E. Moerner, *Biophys. J.* **2001**, *81*, 2851 – 2863.
[61] W. Göhde, Jr., U. C. Fischer, H. Fuchs, J. Tittel, T. Basché, C. Bräuchle, A. Herrmann, K. Müllen, *J. Phys. Chem. A* **1998**, *102*, 9109 – 9116.
[62] a) T. Ha, J. Glass, T. Enderle, D. S. Chemla, S. Weiss, *Phys. Rev. Lett.* **1998**, *80*, 2093 – 2096; b) T. Ha, T. A. Laurence, D. S. Chemla, S. Weiss, *J. Phys. Chem. B* **1999**, *103*, 6839 – 6850.
[63] B. C. Stevens, T. Ha, *J. Chem. Phys.* **2004**, *120*, 3030 – 3039.
[64] a) K. Adachi, R. Yasuda, H. Noji, H. Itoh, Y. Harada, M. Yoshida, K. Kinosita, Jr., *Proc. Natl. Acad. Sci. USA* **2000**, *97*, 7243 – 7247; b) J. E. T. Corrie, B. D. Brandmeier, R. E. Ferguson, D. R. Trentham, J. Kendrick-Jones, S. C. Hopkins, U. A. van der Heide, Y. E. Goldman, C. Sabido-David, R. E. Dale, S. Criddle, M. Irving, *Nature* **1999**, *400*, 425 – 430; c) D. M. Warshaw, E. Hayes, D. Gaffney, A.-M. Lauzon, J. Wu, G. Kennedy, K. Trybus, S. Lowey, C. Berger, *Proc. Natl. Acad. Sci. USA* **1998**, *95*, 8034 – 8039; d) J. N. Forkey, M. E. Quinlan, M. A. Shaw, J. E. T. Corrie, Y. E. Goldman, *Nature* **2003**, *422*, 399 – 404; e) I. Sase, H. Miyata, S. Ishiwata, K. Kinosita, Jr., *Proc. Natl. Acad. Sci. USA* **1997**, *94*, 5646 – 5650.
[65] S. A. Empedocles, R. Neuhauser, M. G. Bawendi, *Nature* **1999**, *399*, 126 – 130.
[66] J. T. Fourkas, *Opt. Lett.* **2001**, *26*, 211 – 213.
[67] C.-Y. Lu, D. A. Vanden Bout, *J. Chem. Phys.* **2008**, *128*, 244501.
[68] J. Hohlbein, C. G. Hübner, *Appl. Phys. Lett.* **2005**, *86*, 121104.
[69] A. Débarre, R. Jaffiol, C. Julien, D. Nutarelli, A. Richard, P. Tchénio, F. Chaput, J.-P. Boilot, *Eur. Phys. J. D* **2004**, *28*, 67 – 77.
[70] M. Prummer, B. Sick, B. Hecht, U. P. Wild, *J. Chem. Phys.* **2003**, *118*, 9824 – 9829.
[71] C. G. Hübner, V. Ksenofontov, F. Nolde, K. Müllen, T. Basché, *J. Chem. Phys.* **2004**, *120*, 10867 – 10870.
[72] a) P. Dedecker, B. Muls, J. Hofkens, J. Enderlein, J.-i. Hotta, *Opt. Express* **2007**, *15*, 3372 – 3383; b) V. Westphal, L. Kastrup, S. W. Hell, *Appl. Phys. B* **2003**, *77*, 377 – 380.
[73] J. Waluk, E. Vogel, *J. Phys. Chem.* **1994**, *98*, 4530 – 4535.
[74] A. V. Failla, S. Jäger, T. Züchner, M. Steiner, A. J. Meixner, *Opt. Express* **2007**, *15*, 8532 – 8542.
[75] a) J. S. Batchelder, M. A. Taubenblatt, International Business Machines Corporation (Armonk, NY), U.S., **1991**; b) L. Novotny, R. D. Grober, K. Karrai, *Opt. Lett.* **2001**, *26*, 789 – 791.
[76] K. J. Vahala, *Nature* **2003**, *424*, 839 – 846.
[77] M. Steiner, A. V. Failla, A. Hartschuh, F. Schleifenbaum, C. Stupperich, A. J. Meixner, *New J. Phys.* **2008**, *10*, 123017.
[78] R. Gutbrod, D. Khoptyar, M. Steiner, A. M. Chizhik, A. I. Chizhik, S. Bär, A. J. Meixner, *Nano Lett.* **2010**, *10*, 504 – 508.
[79] A. Ashkin, *Phys. Rev. Lett.* **1970**, *24*, 156 – 159.
[80] a) A. L. Migdall, J. V. Prodan, W. D. Phillips, T. H. Bergeman, H. J. Metcalf, *Phys. Rev. Lett.* **1985**, *54*, 2596 – 2599; b) S. Chu, J. E. Bjorkholm, A. Ashkin, A. Cable, *Phys. Rev. Lett.* **1986**, *57*, 314 – 317; c) V. S. Bagnato, G. P. Lafyatis, A. G. Martin, E. L. Raab, R. N. Ahmad-Bitar, D. E. Pritchard, *Phys. Rev. Lett.* **1987**, *58*, 2194 – 2197.
[81] a) A. Ashkin, *Biophys. J.* **1992**, *61*, 569 – 582; b) A. Ashkin, *Proc. Natl. Acad. Sci. USA* **1997**, *94*, 4853 – 4860.
[82] A. Ashkin, J. M. Dziedzic, *Science* **1987**, *235*, 1517 – 1520.
[83] A. Ashkin, J. M. Dziedzic, T. Yamane, *Nature* **1987**, *330*, 769 – 771.
[84] K. C. Neuman, S. M. Block, *Rev. Sci. Instrum.* **2004**, *75*, 2787 – 2809.
[85] a) Q. Zhan, *Opt. Express* **2004**, *12*, 3377 – 3382; b) H. Kawauchi, K. Yonezawa, Y. Kozawa, S. Sato, *Opt. Lett.* **2007**, *32*, 1839 – 1841; c) T. A. Nieminen, N. R. Heckenberg, H. Rubinsztein-Dunlop, *Opt. Lett.* **2008**, *33*, 122 – 124; d) D. W. Zhang, X.-C. Yuan, *Opt. Lett.* **2003**, *28*, 740 – 742.
[86] S. Yan, B. Yao, *Phys. Rev. A* **2007**, *76*, 053836.
[87] A. T. O'Neil, M. J. Padgett, *Opt. Commun.* **2001**, *193*, 45 – 50.
[88] M. E. J. Friese, T. A. Nieminen, N. R. Heckenberg, H. Rubinsztein-Dunlop, *Nature* **1998**, *394*, 348 – 350.
[89] M. Fleischer, C. Stanciu, F. Stade, J. Stadler, K. Braun, A. Heeren, M. Häffner, D. P. Kern, A. J. Meixner, *Appl. Phys. Lett.* **2008**, *93*, 111114.
[90] a) A. Bouhelier, *Microsc. Res. Tech.* **2006**, *69*, 563 – 579; b) L. Novotny, S. J. Stranick, *Annu. Rev. Phys. Chem.* **2006**, *57*, 303 – 331; c) *Tip Enhancement (Advances in Nano-Optics and Nano-Photonics)* (Eds.: S. Kawata, V. M. Shalaev), Elsevier, Amsterdam, **2007**.
[91] J. Homola, S. S. Yee, G. Gauglitz, *Sens. Actuators B* **1999**, *54*, 3 – 15.
[92] B. Rothenhäusler, W. Knoll, *Nature* **1988**, *332*, 615 – 617.
[93] a) C. E. H. Berger, R. P. H. Kooyman, J. Greve, *Rev. Sci. Instrum.* **1994**, *65*, 2829 – 2836; b) W. Hickel, W. Knoll, *Thin Solid Films* **1990**, *187*, 349 – 356.
[94] K. Watanabe, G. Terakado, H. Kano, *Opt. Lett.* **2009**, *34*, 1180 – 1182.
[95] K. J. Moh, X.-C. Yuan, J. Bu, S. W. Zhu, B. Z. Gao, *Opt. Lett.* **2009**, *34*, 971 – 973.
[96] D. P. Biss, T. G. Brown, *Opt. Lett.* **2003**, *28*, 923 – 925.
[97] M. Hashimoto, K. Ashida, K. Yoshiki, T. Araki, *Opt. Lett.* **2009**, *34*, 1423 – 1425.
[98] E. Y. S. Yew, C. J. R. Sheppard, *Opt. Commun.* **2007**, *275*, 453 – 457.
[99] S. Yang, Q. Zhan, *J. Opt. A Opt.* **2008**, *10*, 125103.
[100] H. Dehez, M. Piché, Y. De Koninck, *Opt. Lett.* **2009**, *34*, 3601 – 3603.
[101] D. Ivanov, V. Shcheslavskiy, I. Märki, M. Leutenegger, T. Lasser, *Appl. Phys. Lett.* **2009**, *94*, 083902.
[102] A. V. Nesterov, V. G. Niziev, *J. Phys. D* **2000**, *33*, 1817 – 1822.
[103] K. Venkatakrishnan, B. Tan, *J. Micromech. Microeng.* **2006**, *16*, 2603 – 2607.
[104] B. R. Boruah, M. A. A. Neil, *Rev. Sci. Instrum.* **2009**, *80*, 013705.

